Speciation studies at the Illite - solution interface: Part 1 – Sorption of phosphate ions

Shang Yao Guo, Mirella Del Nero, Olivier Courson, Sylvia Meyer-Georg, Rémi Barillon

Speciation studies at the Illite - solution interface: Part 1 - Sorption of phosphate ions

Shang Yao Guo, Mirella Del Nero*, Olivier Courson, Sylvia Meyer-Georg, Rémi Barillon

Institut Pluridisciplinaire Hubert Curien, UMR 7178 Université de Strasbourg/CNRS - IPHC, 23 rue du Loess 67037 Strasbourg, France

*Corresponding author. E-mail address: mireille.delnero@iphc.cnrs.fr - Phone: +33 03 88 10 64 08

Abstract

Although phosphate ion (hereafter "P") sorption is known to influence clay surface reactivity and trace metal behavior in the environment, there is still a lack of in situ spectroscopic evidence on the identity of phosphate sorption species formed at the interface between solution and clays with a 2:1 layered structure (2 silica tetrahedral: 1octahedral layers), which are ubiquitous in soils and clay formations. We studied the surface speciation of phosphate ions by in situ spectroscopic monitoring along P sorption at the interface between a solution and a homoionic Na-illite, as a function of time or aqueous phosphate concentrations (20-250µM) leading to low/moderate P surface coverage. We also combined them with batch sorption experiments and electrophoretic mobility (EM) measurements. Macroscopic data indicated that the percentage of P sorption depends on pH, aqueous phosphate concentration, and the clay/solution ratio of the experiment, *i.e.*, the coverage of the clay surface by P, with a maximal sorption capacity of the clay equal to ca. 6 $\mu mol.g^{-1}$ at pH 4. Macroscopic and EM data further suggest that P sorption mechanisms onto illite confer negative charges on the surface and involve several sorption species and/or surface sites present on the clay edges. In situ FTIR spectra showed that, at acidic pH, three types of phosphate surface species exist at the illite-solution interface: an outer-sphere surface complex (OSSC) of phosphate ($\Xi SOH_2^+ \ldots H_2PO_4^-$, with S referring to a sorption site on the clay), an inner-sphere surface complex (ISSC) of phosphate, probably a monodentate binuclear surface complex ($(\Xi SO)_2PO_2$) formed by surface ligand exchange with high-affinity aluminol sites and, to a lesser extent, low-affinity sites on the clay edges, and, in limited amounts, an Al-phosphate surface precipitate. Phosphate ion sorption occurs through the initial formation of the OSSC of phosphate, which dominates phosphate surface speciation at short reaction times and low P concentrations and transforms over time into the ISSC of phosphate. This study presents the first published in situ surface speciation of phosphate ions sorbed at the interface between a solution and an illite. The evidence of a strong sorption of

phosphate ions at this clay surface provides new and sound knowledge to better understand the environmental fate of phosphate ions and trace metals, particularly in agricultural soil - groundwater continua or in clay host rocks considered for high-level radioactive waste disposal.

Keywords

Illite / Phosphate sorption / Surface speciation / Clay-solution interface / In situ monitoring / Attenuated Total Reflexion Fourier Transform InfraRed Spectrocopy / Environment.

1 Introduction

The sorption of phosphate ions (hereafter "P") onto minerals is linked to major issues of ecosystem health and functioning, such as the regulation of P mobility in (ground)waters, - particularly in the case of an excessive application of P-containing fertilizers to soils-. It has long been reported that phosphate ions have a strong ability to bind on the surfaces of iron or aluminum (oxihydr)oxides[1–15] and, to a lesser extent, clays [12–14,16–23], which are common minerals in soils and sediments. Furthermore, the high phosphorous-binding capacity of sediments and soils is reported to be correlated with their high clay mineral content (cf. [12]). While many spectroscopic studies have focused on the speciation of P sorbed to the surface of iron or aluminum (oxihydr)oxides [3–11,15], far fewer have been devoted to P sorbed onto clays [13,19–21,23] and detailed knowledge on the sorption mechanisms and species involved is still lacking. Therefore, further work is needed to obtain spectroscopic data on the in situ speciation of sorbed phosphate ions at the interfaces between solution and clay, on which to base a complete understanding and robust predictions of P behavior in soil-water continuums.

Other main environmental issues related to P sorption concerns the behavior of trace metal elements (TME), in particular rare earth elements (REE) and uranium (U), e.g., their fate in the vicinity of U ores/mines [24,25], their soil stabilization by P injections [26,27], and the trapping properties of host clay rocks for disposal of high level radioactive wastes [28–31]. It is well

known that phosphate ions have a high chemical affinity for REE [32] and U in its potentially-mobile hexavalent state [33–36]. Depending on experimental conditions, P was found to increase the solubility of these TME through formation of aqueous complexes [33] or limit it through formation of U/REE-phosphate (co)precipitates [33,37–43], and/or to be involved in TME-phosphato surface species sorbed to surfaces of Fe-(oxihydr)oxides and Al-(oxihydr)oxides [44,45] or clays [44,46–48]. Field studies have also supported the formation of U/REE-phosphate co-precipitates [43,49–58] in the vicinity of U ore deposits, and have highlighted that U/REE, phosphate and Fe/Al-(oxihydr)oxides [52,59–65] or clays [60,61,65] can exist in close association in P-rich soils and sediments. Hence, acquiring spectroscopic evidence of P surface speciation onto clays is of paramount importance to provide a sound background and fundamental understanding of TME sorption behavior in soil –water systems, where phosphate ions are ubiquitous and can affect the TME sorption through competitive and / or synergistic processes, e.g. through a control of clay surface reactivity [66] and/or by competing or co-sorbing with TME on clay sorption sites [46,48]. Experimental studies have indeed reported that the sorption of P promotes the retention of U onto kaolinite at acidic to neutral pH [67] but has no macroscopic signature on U sorption on montmorillonite [46], which first raises the question of the surface properties of clays on P surface speciation.

The objective of this study is to provide new insights into the sorption of phosphate ions at the interface between solution and a pure illite surface, by acquiring novel spectroscopic data from in situ monitoring of the clay–solution interface by using a state-of-the –art technique, Attenuated Total Reflection Fourier Transform Infrared Spectroscopy (ATR FTIR). Several studies have long suggested that phosphate ions are sorbed at clay surfaces as inner-sphere surface complexes (ISSC) of phosphate formed on clay surface sites, as presented in detail in the bibliographic review by Arai and Spark [68], -and mainly on sites existing on the alumina-like clay layers [14,18,22]-, and that the P sorption decreases with pH and the progressive

84 deprotonation of clay surface hydroxyl groups that is unfavorable to the electrostatic attraction
85 of phosphate anions existing in solutions at pH 4-8. However, several papers have highlighted
86 that important parameters are the content of minor phases like metal-(oxihydr)oxides acting as
87 strong sorbents of P in clay rocks and / or the presence of sorbed cations (e.g., Fe, Al and Ca)
88 bridging P sorbed to the clay surfaces [18,22,23,47]. Moreover, several mechanistic studies
89 aiming at elucidating the identity of P surface species have focused on non-purified clays and/or
90 on the simultaneous sorption of P and TME. For example, Borgnino et al. [23] have performed
91 sorption experiments of phosphate ions at the surface of a Fe-modified montmorillonite. These
92 authors have evidenced by using in situ ATR FTIR spectroscopy the formation of multiple, pH-
93 dependent phosphate surface complexes at mineral–water interfaces but they have indicated
94 that the sorption took place onto Fe-(hydr)oxides pre-existing in the clay sample studied, rather
95 than on the surface of montmorillonite itself. Phosphate ions sorbed onto a La-modified
96 bentonite were shown to be immobilized as a rhabdophane phase ($LaPO_4 \cdot n\ HO_2$) by Extended
97 X-Ray Absorption Fine Structure (EXAFS) and ^{31}P solid-state Nuclear Magnetic Resonance
98 (NMR) analyses [48]. Troyer et al. [46] have investigated by EXAFS the effect of phosphate
99 ions on U(VI) uptake by montmorillonite and have shown that formation of uranyl phosphato
100 ternary surface species has occurred without a macroscopic signature of P sorption, which was
101 attributed to a low binding of phosphate ions in the absence of U(VI).

102 Actually, to our best knowledge, only two spectroscopic studies have aimed at establishing the
103 speciation of phosphate ions sorbed at a pure clay mineral surface. Van Emmerik et al. [13]
104 conducted ^{31}P solid-state NMR investigations on the sorption of phosphate ions at the surface
105 of kaolinite. They found that P was sorbed via a combination of reactions of formation of
106 phosphate ISSC, which involve singly-coordinated Al-OH sites at the clay edge, and surface
107 precipitates of $AlPO_4$. Due to the technique used, their study was more focused on high
108 phosphate surface loading conditions and ex-situ surface speciation measurements, for which

previous studies have raised a possibility of speciation change upon solid drying [7]. A recent in situ ATR FTIR spectroscopy work on P sorbed at the kaolinite–water interface has confirmed the formation of (possibly multiple) ISSC of phosphate onto surface sites of kaolinite [19], likely aluminol sites, but the authors have underlined that a detailed investigation of P surface speciation was beyond the purpose of their study mainly devoted to the competitive phosphate – oxytetracycline sorption. Further extensive and in situ spectroscopic work is therefore necessary to elucidate the identity of phosphate surface species formed at low to moderate P loading at clay-solution interfaces, -particularly for 2:1 layered clays for which no in situ spectroscopy studies of P surface speciation have been reported to date-.

In this study, we sought to provide clear spectroscopic evidence to fully identify the multiple phosphate sorption species formed at the interface between solution and pure illite, when increasing reaction time or phosphate surface coverage from low to moderate (< 6 µmol.g^{-1}). These two key parameters have long been shown to control P sorption mechanisms on iron and aluminum (oxihydr)oxides ([69–71]). ATR FTIR spectroscopy experiments were performed to record in situ the P-O stretching vibration modes of phosphate units sorbed at the interface between solution and a pure homoionic Na-illite, along the process of P sorption and / or an increase in P loading. ATR FTIR spectroscopy technique has several advantages: (i) it has an increased sensitivity for sorbed species [66,72], (ii) it is powerful to study the speciation of oxyanions sorbed at the interface [72], and (iii) it allows in situ monitoring of multiple surface species [8,73]. Complementary batch sorption experiments were also carried out to characterize the effects of solid-to-liquid ratio ($R_{S/L}$: 1-3 g.L^{-1}), pH (4-8) and total concentration of phosphate ions ($[P]_{I,aq}$: 0-250µM) on the macroscopic P sorption. Electrophoretic mobility (EM) measurements of the experimental clay suspensions were made in order to provide indirect information on the surface charges imparted to the clay surface by sorption reactions of phosphate species. To our knowledge, this study presents the first published in situ surface

speciation of the phosphate ion at the illite-solution interface, for P concentrations relevant to natural water-clay systems, and gives valuable insights into the mechanisms of phosphate sorption on a 2:1 layered clay. The results presented here have environmental implications, as they provide a necessary basis for a better understanding of the interactions that can occur in complex illite-phosphate-TME systems, which are relevant to soils and clay formations considered for HLW repositories (e.g. Callovo-Oxfordian and Opalinous clays), in which illite is a principal mineral phase.

2 Materials and methods

2.1 Source materials

All the solutions used in experiments were prepared by using ultrapure Milli-Q water (purity > 18 MΩ.cm) and reagent grade chemicals. The source material is an argillaceous clay ("Illite du Puy"), which is collected in the region of Le Puy-en-Velay in the Massif Central Mountains in France and is provided by the company "Argile Verte du Velay". Two clay stock samples were used. The first one (hereafter "IdP") corresponds to the particle size fraction lower than 77 µm of the Illite du Puy source material and it was used in the experiments as received. The second stock sample (hereafter "NaIdP") was obtained by purification of a subsample of IdP in order to convert the initial illite into a Na-homoionic illite. The subsample was conditioned by acid washing and subsequent exchange of the exchangeable cations against Na^+ by using the method detailed by Glaus et al. [74]. The treatment is also expected to remove hydrolyzed products -such as hydroxy-aluminum compounds-, phosphate impurities and soluble minerals like calcite [30,74]. Briefly, a multistep conditioning procedure was carried out as follows. An IdP subsample (50 g) was brought in contact with a known volume (1 L) of a 1M NaCl/0.1M formate buffer (FB) solution (with FB being a 0.05 M Na-formate - 0.05 M formic acid solution at pH 3.5, and the solid-to-liquid ratio, being equal to 50 $g.L^{-1}$). After a 4-hours equilibration of the clay suspension by gentle stirring, the particles were left to settle overnight by sedimentation.

159 The supernatant solution was then removed and the particles were re-suspended by addition (to
160 1 L) of a 1 M NaCl / 0.1 M FB solution (ratio: 50 $g.L^{-1}$). The procedure described above was
161 repeated six times in order to largely remove acid-soluble Ca^{2+}-mineral phases, too. Remaining
162 solid was then washed three times by 0.1 M NaCl in order to remove format buffer, exchanged
163 cations and solubilized impurities. It was filled into dialysis bags (Visking® dialysis tubing,
164 MWCO: 12-14 kDa, Pore diameter: ca. 25 Å, SERVA, Heidelberg, Germany) and dialyzed
165 with a "clay water" prepared as follows. A subsample of 1g of IdP was brought in contact with
166 10mL of Milli-Q® water in a dialysis bag. The dialysis bag was then equilibrated with 3 L of
167 Milli-Q® water during 24 h and the concentration of Na^+ in the external solution was measured.
168 The external solution was removed and refilled with Milli-Q® water until the concentration of
169 Na^+ in the external solution dropped to < 1 mM. This external dialyzed solution was called
170 "clay water". The final solid sample was dried at 40°C and then powdered in an agate mortar
171 and sieved. The size fraction < 75 µm was selected and taken as the final NaIdP stock sample,
172 which was stored in a desiccator until its use in experiment.

173 *2.2 Characterization of Illite du Puy*

174 2.2.1 Mineralogical and chemical analyses

175 The mineralogical compositions of IdP and NaIdP were obtained from X-ray diffraction (XRD)
176 analyses conducted with a Bruker diffractometer (D8 Advance Eco) at the ITES Institute
177 (Institut Terre et Environnement de Strasbourg, France). The measurements were performed on
178 both the whole-rock samples and their clay size fraction. The fraction of size lower than 2 µm
179 that was recovered by centrifugation of the suspensions (at 1000rpm during 2 min. using a
180 Heareus Megafuge 40R centrifuge and based on calculations using Stockes' law). It was
181 isolated by settling, oriented on glass slides and XRD analyses were performed on the sample:
182 a) without any treatment, b) after sample saturation overnight in ethylene-glycol (EG), c) after
183 sample heating at 490°C for 4 h, and d) after sample saturation overnight in hydrazine [75].

184 Clay minerals constitutive of the clay size fraction were then identified by values of their layer
185 and interlayer spacing deduced from diffractograms [76]. A semi-quantitative estimate of the
186 percentage of each clay mineral was made by using the software DIFFRAC.EVA version 4.3,
187 with an error in reproducibility of the measurements of less than 5 % for each mineral. Chemical
188 analyses of IdP and NaIdP, and their respective clay size fraction, were conducted at SARM-
189 CRPG (Service d'Analyse des Roches et Minéraux, Centre de Recherches Pétrographiques et
190 Géochimiques, Nancy, France). Major and trace element analyses were made by using a
191 Thermo Fischer ICap 6500 inductively coupled plasma optical emission spectrometer (ICP-
192 OES) and a Thermo Elemental X7 inductively coupled plasma mass spectrometer (ICP-MS),
193 respectively. The analytical error depends on an element concentration, and was determined to
194 be lower than 0.1 % (weight % oxides) and in the range 5-20 % for ICP-OES and ICP-MS
195 measurements, respectively (< 10 % for U concentrations > 10 $\mu g.g^{-1}$).

196 2.2.2 Specific surface area

197 Specific surface areas of IdP and NaIdP samples were determined by N_2-BET measurements
198 using an ASAP2420 surface area and porosity analyzer. Subsamples were degassed for 4 h at
199 150°C before measurements. Values of specific surface areas were found to be equal to 92 and
200 107 $m^2.g^{-1}$ for IdP and NaIdP, respectively. These values are in good agreement with the value
201 (97 $m^2.g^{-1}$) obtained by Bradbury and Baeyens [77].

202 2.2.3 Preliminary experiments of (Na)IdP-solution interactions

203 Preliminary experiments were conducted in order to determine the chemical evolution of a
204 solution brought in contact with IdP or NaIdP, respectively, as function of key physicochemical
205 parameters. Batch experiments were performed under atmospheric conditions and at a defined
206 ionic strength value (0.005 M NaCl), for varying values of solid-to-solution ratio, $R_{S/L}$ (from
207 0.5 to 6 $g.L^{-1}$ and 0.5 to 3$g.L^{-1}$ for IdP and NaIdP, respectively), reaction time, t_R (24 hours - 7
208 days), and pH (3-7). Suspensions of (Na)IdP were prepared in individual (50mL) polypropylene

tubes at desired values of $R_{S/L}$ and initial pH (2.3 to 3.8 for IdP and 2.7 to 6.2 for NaIdP). The suspensions were then equilibrated by gently shaking end-over-end during a desired reaction time (from 2 hours to 4 days). Final pH was measured (uncertainty: 0.05 pH unit). After the equilibration step, the suspensions were centrifuged for a solid–solution separation at 9000 rpm for 3 hours (which led to a separation threshold of ca.16 nm for illite, based on calculations using Stockes' law). Ultrafiltration tests of two centrifuged solutions were also carried out by passing subsamples of the centrifuged supernatant through a 3kDa-filter (Centricon filter) and were taken for TME analysis. A defined volume of supernatant solution was taken from each individual tube and was acidified at pH < 1 by adding a small amount of 67% HNO_3 for analysis of major and trace elements by ICP-OES (Varian 720es) and ICP-MS (Agilent 7700x), respectively (uncertainty ranges of 2-20 % and 5-20 %, respectively). The analyses were performed at the Department of Analytical Sciences of IPHC (Strasbourg, France).

2.3 Macroscopic sorption of phosphate ions

2.3.1 Experimental procedure

Batch sorption experiments were carried out at 25°C under atmospheric conditions to evaluate the effect of pH, total concentration of phosphate ions (noted $[P]_{I,aq}$), and solid-to-solution ratio ($R_{S/L}$) on the retention of phosphate ions at the NaIdP–solution interface. Batch experiments (performed in 0.005 M NaCl electrolyte solutions) were carried out to obtain: (i) phosphate sorption edges (range of final pH, pH_F, of 3-8) at various $R_{S/L}$ (1, 2 or 3 $g.L^{-1}$, $[P]_{I,aq}$: 20 µM), (ii) sorption edges at two phosphate concentrations (20 µM and 100 µM, $R_{S/L}$: $3g.L^{-1}$) and (iii) phosphate sorption isotherms at pH 4 ($[P]_{I,aq}$: 20-200 µM, $R_{S/L}$: $3g.L^{-1}$). The experiments were conducted as follows. Suspensions of NaIdP in 0.005 M NaCl electrolyte solutions were pre-equilibrated for 3 days in 15 mL polypropylene centrifuge tubes, at desired values of $R_{S/L}$ and pH. If necessary, solution pH was adjusted during pre-equilibration by adding very small volumes of a 0.1 M HCl or 0.1 M NaOH solution. After 3 days of pre-equilibration, an aliquot

of a stock phosphate solution of 0.05 M was added in the tubes to achieve the desired $[P]_{I,aq}$ value and the tubes were gently shaken end-over-end for 4 days. Final pH was measured after a 4-days contact time of sorbate–suspension. Separation between solid and solution phases was carried out by centrifugation of the suspensions for 3 hours at 9000 rpm (which led to a separation threshold of ca.16 nm for illite, based on calculations using the Stockes' formula). The supernatants were then removed from the tubes after centrifugation. An aliquot was taken for electrophoretic mobility (hereafter "EM") measurements. Another aliquot was taken for chemical analyses after acidification at pH < 1 by addition of 2% HNO_3. Each experiment was performed in duplicate. Blank experiments were also carried out in a similar manner than described above except that no clay was added in the tubes.

2.3.2 Analysis of experimental solutions of sorption experiments

Measurements of EM of suspended particles present in supernatant aliquots collected at the end of the sorption experiments were made by using a Zetasizer Nano equipment (Malvern). Each sample was measured three times and the standard error was then calculated. Quantitative analysis of final aqueous phosphate concentrations ($[P]_{F,aq}$) in supernatant aliquots (re-filtered at 0.20 µm) were made by ion chromatography (Eco IC, Metrohm, uncertainties of 1 – 10%). An aliquot of each supernatant was also acidified to pH < 1 by adding a small amount of 67% HNO_3 and it was stored at 4°C prior to further chemical analyses. Percentages of P sorbed, and amount of P sorbed (in µmol.g^{-1} clay), were calculated as follows:

$$\%\ P\ sorbed = \frac{[P]_{I,aq} - [P]_{F,aq}}{[P]_{I,aq}} \times 100$$

$$Amount\ P\ sorbed\ (\mu mol/g) = ([P]_{I,aq} - [P]_{F,aq}) \times \frac{V}{M}$$

With $[P]_{I,aq.}$: initial aqueous concentration of sorbate (µmol.L^{-1}), $[P]_{F,aq}$: final aqueous concentration of sorbate (µmol.L^{-1}), V: volume of liquid (L) and M: mass of solid phase (g).

Uncertainties on the sorption percentage and surface coverage were estimated to be lower than 10%.

2.4 In situ ATR FTIR experiments

2.4.1 Procedures of clay deposition on the ATR crystal

Acquisition of IR spectra at the mineral-solution interface was carried out by using a Bruker Equinox IFS 55 infrared spectrometer equipped with an ATR cell containing a ZnSe horizontal crystal (with an angle of incidence of 45°, a crystal size of 7.2×1.0×0.7 cm^3 and 5 internal reflections) and with a MCT detector (system cutoff: ca. 900 cm^{-1}) that was cooled down by liquid nitrogen during FTIR spectra acquisition. Prior to experiment, the ZnSe crystal was either coated with a thin and stable film of IdP or NaIdP brought subsequently in contact with a 0.005 M NaCl electrolyte, or it was directly brought in contact with a previously pre-equilibrated NaIdP suspension from which the clay particles are left to settle and cover the crystal. Both methods have the advantage of allowing an in situ monitoring of the solid–solution interface.

The former method was shown in previous studies to be powerful to monitor sorbate sorption at aluminum oxide–solution interface, with a good reproducibility of the FTIR sorption experiments and an increased sensitivity of the technique for surface species [8,73]. It was used in the present work to gain IR reference data on the structure of the clay samples studied and / or on surface hydroxyls present at clay – solution interface (cf. §2.4.2), by monitoring of interface between IdP and NaIdP samples and a not equilibrated electrolyte solution. It was conducted by using a multistep procedure as follows : (i) an IdP or NaIdP suspension was prepared (contact time : 0.5 h, $R_{S/L}$=5 $g.L^{-1}$, initial pH 4, respectively) and particles were left to settle by sedimentation during 1 hour, (ii) ca. 2mL of the supernatant were then pipetted, deposited uniformly onto the ZnSe crystal surface, and let to dry overnight at room temperature (25°C) for settling of particles, (iii) the crystal was dried at 40°C for 3 hours, and (iv) the coating

281 obtained after drying was gently rinsed with an electrolyte at a pH similar to that of the initial
282 suspension and dried slowly under a N_2 gas flow. The whole procedure described above was
283 repeated for four times. This procedure was found to be repeatable and it allowed to deposit a
284 thin film of ca.3 mg of solid onto the crystal.

285 The latter method, i.e., covering of the ATR crystal with an equilibrated NaIdP–electrolyte
286 solution bilayer system, was used to monitor by in situ ATR FTIR spectroscopy the sorption of
287 phosphate ions at the interface (cf. §2.4.4), for nearly equilibrated systems prepared to avoid
288 any significant contribution from clay dissolution to the IR signal and / or structural
289 reorganization / formation with time of surface hydroxyl groups at the clay-solution interface
290 (cf. §2.4.3). It was conducted as follows: (i) a NaIdP-0.005M electrolyte suspension was
291 prepared in a polypropylene tube and left to pre-equilibrate by gently shaking end-over-end of
292 the tube during a contact time of 3 days ($R_{S/L}$= 3 $g.L^{-1}$, pH 4), (ii) 10mL of the suspension were
293 then pipetted and added into the ATR cell, (iii) the suspension was left to settle on the ATR
294 crystal for 3 days and (iv) an ATR FTIR spectrum was taken as a reference baseline.

295 2.4.2 Monitoring of the clay-solution interaction

296 In situ ATR FTIR spectroscopy experiments were performed to monitor the clay–solution
297 interface during interaction of (Na)IdP with a not equilibrated NaCl electrolyte solution, with
298 the purpose of gaining insights into IR vibrations originating from surface hydroxyl groups at
299 the interface and / or clay structure (as structural reorganizations of the solid sample are likely
300 during the interaction). After coating of the ATR crystal with a dried thin film of IdP or NaIdP
301 (cf. §2.4.1), the film was brought in contact with a volume of 10mL of a 0.005 M NaCl
302 electrolyte solution in the ATR cell, in order to perform FTIR measurements of the (Na)IdP–
303 solution interface (initial pH: 4, final pH: 6.2 for IdP and 4 for NaIdP). A FTIR spectrum was
304 immediately recorded as a reference baseline after electrolyte addition. The (Na)IdP-solution

interaction process was then monitored during 3 hours. Each IR spectrum was recorded during 20min with an average of 2000 scans/spectrum at a resolution of 4 cm^{-1}.

2.4.3 Blank ATR-FTIR experiment: monitoring of an equilibrated NaIdP-solution interface

An ATR FTIR experiment was performed to monitor in situ the evolution of the interface between NaIdP and a nearly equilibrated electrolyte solution at pH 4, in order to ensure a poor contribution to FTIR interface spectra of IR vibration bands originating from formation / structural reorganization with time of hydroxyl groups existing at the clay surface ("blank experiment"). These IR vibration bands must be identified as they may possibly interfere, on ATR FTIR interface spectra recorded during experiments of phosphate ion sorption, with the IR signal originating from the sorbed PO_4 units, in the wavenumber's range 900-1200cm^{-1}. The blank experiment was conducted as follows. After covering of the ATR crystal by a nearly equilibrated NaIdP-electrolyte solution bilayer system as described in §2.4.1, and after an immediate recording of a first FTIR spectrum as a reference baseline, the NaIdP-solution interface was monitored during a reaction time of 3 days. Each IR spectrum was recorded during 20min with an average of 2000 scans/spectrum at a resolution of 4 cm^{-1}. There was observed the appearance of a weal IR signal in the wavenumber range 1000-1200cm^{-1} and its limited growth with time. The weak IR signal was attributed to a very limited formation / structural reorganization of surface hydroxyls on clays with time. This signal was proven negligible compared to the IR signals acquired during the ATR FTIR phosphate sorption experiments (cf. §3.4.3). This blank experiment therefore confirmed that the preparation procedure of the NaIdP-solution bilayer system (3 days of pre-equilibration followed by 3 days of NaIdP particles settling form the pre-equilibrated suspension on the ATR crystal) was appropriate to ensure a nearly equilibration of the NaIdP – electrolyte solution interface before the start of the ATR FTIR phosphate sorption experiment.

2.4.4 Monitoring of the clay–solution interface along sorption of phosphate ions

Experiments were performed to monitor in situ the sorption of phosphate ions at the interface between NaIdP and a nearly equilibrated electrolyte solution, and to gain insights into IR vibration bands of phosphate sorption species. Two types of ATR FTIR experiments of sorption of phosphate ions were performed. The first one was devoted to monitor the NaIdP-phosphate-solution interface as a function of reaction time, for a $[P]_{I,aq}$ value of 100µM and a pH value of 4. It was conducted as follows. After covering of the ATR crystal with the nearly equilibrated NaIdP-electrolyte solution bilayer system and recording of a FTIR spectrum as a reference baseline (cf. §2.4.1), a defined amount of a stock phosphate solution was added into the ATR cell in order to achieve a $[P]_{I,aq}$ value of 50 µM. IR spectra of the interface were then recorded during 1 hour (one spectrum per 20 min.). Total concentration of aqueous P added was then increased to 100µM by the introduction of an appropriate amount of the stock phosphate solution in the cell. The IR spectra of the interface were then collected as a function of reaction time (t_R up to 3 days). The second ATR FTIR experiment aimed at investigating the NaIdP-solution interface during a continuous increasing of the $[P]_{I,aq}$ value from 100 µM to 300 µM. The experiment was performed as described previously up to the collection of IR spectra at $[P]_{I,aq}$ of 100 µM, for a t_R value equal to ca. 19 h, which was previously shown to allow the appearance of a strong IR signal originating from ISSC of sorbed phosphate (based on FTIR results of the above-mentioned first-type experiment). The total concentration of phosphate was then raised from 100 to 300 µM by successive additions of 50 µM of phosphate ions, at a rate of one addition per hour. IR spectra were collected immediately after each increase of the aqueous phosphate concentration, and then every twenty minutes.

2.4.5 FTIR spectra of aqueous phosphate species

Supporting Information reports the calculated aqueous speciation of P(V) in 0.005M NaCl electrolyte solutions (Fig. S1), and the equilibrium constants used for calculations (Table S1).

Aqueous phosphate species existing in these solutions are the triply protonated (H_3PO_4) phosphate ion (pH <4), the diprotonated monovalent phosphate ion, $H_2PO_4^-$, as a main species in the pH range 3-6, and the monoprotonated (HPO_4^{2-}) phosphate ion (pH >5). Much IR studies have been previously published in the literature on these aqueous species and only a short overview is given here (cf. §1 in Supporting Information). Nevertheless, FTIR measurements (without clay) were performed in the present study for 0.005 M NaCl electrolyte solutions at various pH (4-7) and total aqueous concentrations of phosphate ions ($[P]_{I,aq}$: 20-225 µM), in order to: (i) get values of detection limits of the ATR FTIR technique for aqueous phosphate species, (ii) record IR spectra of aqueous phosphate species to be taken as "references" for the sorption species, -for example, to distinguish between formation of outer-sphere and inner-sphere surface complexes of phosphate-, and (iii) identify a possible formation of phosphate precipitates, depending on experimental conditions. A defined volume of a 0.005 M NaCl electrolyte solution was brought at a desired pH value and was added into the ATR cell. A reference spectrum was taken. Then, a defined volume of the phosphate stock solution was added to the electrolyte solution into the ATR cell in order to attain a defined $[P]_{I,aq}$ value. Total concentration of aqueous P added was then increased by successive additions of defined volumes of the stock phosphate solution. After each addition, one or several spectra were recorded. Phosphate aqueous species, and their detection limits, were studied in the range of $[P]_{I,aq}$ values of 20–225 µM (45–175 µM at pH 4, 50–150 µM at pH 4.9, 30–225 µM at pH 6.2, 20–150 µM at pH 7.0). The IR spectra are given and detailed in Supporting Information (cf. Fig. S2 and §2). In the range of $[P]_{I,aq}$ and pH values investigated in this study, only the υ_3(P-O) bands at 1160 and 1075 cm^{-1} of $H_2PO_4^-$ were observable, and the detection limit for this aqueous species is estimated to be approximately of 45 µM in the pH range 4-6.2. ATR FTIR analyses were also made to determine the IR band positions of aqueous iron(III)–phosphate species, although only low concentrations of Fe^{3+} ions were found to be released in solution

during illite-solution interactions. IR analysis was conducted for a 0.005M solution introduced into the ATR cell, in which desired volumes of stock solutions of Fe(III) and phosphate ions were added simultaneously to achieve target concentrations of Fe(III) and phosphate ions ($[Fe]_{I,aq}$=10µM and $[P]_{I,aq}$=100µM).

2.4.6 Analysis of FTIR spectra

Analyses of FTIR spectra were focused on the 900–1200 cm^{-1} mid-infrared region where bands associated with various P-O(H) stretching vibrations of the phosphate unit, i.e., where υ_3 triply degenerated asymmetric stretching and υ_1 non degenerated symmetric stretching vibration bands, are found [3,6,7,78]. There is also a broad band on IR spectra of $H_2PO_4^-$ and H_3PO_4 aqueous species that has been attributed to the δ(P-OH) bending vibration located at ca. 1220–1240 cm^{-1} [7,11]. The software OriginPro version 9.1 was used for correction of baseline of the FTIR interface spectra. A linear baseline was fitted between 1200 and 900 cm^{-1} on the raw spectra, and was brought to a zero value. The software was also used for the decomposition of the baseline-corrected spectra in order to resolve IR bands with Gaussian lines, and the least-square fitting was applied. No constraints were applied on adjustable parameters (band position, band intensity and band width) during spectral decompositions. The band maxima position was adjusted only for a very few spectra showing low absorbance.

3 Results and discussion

3.1 Chemical and mineralogical compositions of Illite du Puy

The mineralogical compositions of the IdP and NaIdP samples, and of their clay-size fraction (< 2µm), are given in Table 1. Calcite is the major mineral constitutive of IdP, followed by feldspars (mainly potassic) and clays, i.e., illite and kaolinite. Quartz and siderite are present in the sample as minor minerals, and hematite as an accessory mineral. The clay fraction has a quite simple composition dominated by illite, then kaolinite. A striking feature is the

disappearance of the main mineral, i.e., calcite, after Na-homonionic conditioning of illite du Puy. NaIdP is composed mainly by illite and feldspars -and small amounts of kaolinite and quartz-, while no carbonates (calcite, siderite) nor hematite were detected by XRD analysis.

Table 1. Mineralogical composition (semi-quantitative estimate in %, error in reproducibility of measurements: 5%) of IdP and NaIdP samples and their clay fraction (< 2 µm).

	Clay		Carbonate		Feldspar			Iron Oxide	
	Illite	*Kaolinite*	*Calcite*	*Siderite*	*Microcline*	*Orthoclase*	*Albite*	*Hematite*	*Quartz*
IdP	18.5	5.4	32.8	3.3	18.2	11.6	6.3	0.4	3.5
NaIdP	30.2	7.2	-		20.6	20.5	16.6	-	4.9
IdP$_{(<2µm)}$	79	21	-		*Traces*			-	
NaIdP$_{(<2µm)}$	76	24	-		*Traces*			-	

The major element compositions of IdP and NaIdP are given in Table 2 and are consistent with those of silicate rocks whose mineralogy is dominated by K-feldspars, carbonates and clays. Fe_2O_3 represents a significant percentage (> 5%) of the compositions of the two rocks studied, although siderite and hematite cannot be detected in NaIdP by XRD analysis. Iron minerals may therefore represent less than 5% of the mineralogical composition of NaIdP and / or Fe is incorporated in the clay's structure, as proposed by Poinssot et al. [79] for conditioned Na-illite. Removal of carbonate minerals upon clay conditioning is highly marked in the rock compositions by a sharp decrease of the percentage of CaO from IdP to NaIdP. The treatment also led to the removal of traces of phosphate minerals. The chemical composition of NaIdP is consistent with that given for Na-illite by Bradbury and Baeyens [77], whose Na-homoionic conditioning procedure for Illite du Puy has been used in the present study.

Table 2. Major element composition of IdP and NaIdP samples and associated uncertainties (in wt/wt percent oxide). D.L.: detection limit, LOI: loss on ignition.

	SiO_2	Al_2O_3	Fe_2O_3	K_2O	CaO	MgO	TiO_2	P_2O_5	Na_2O	MnO	LOI
IdP	44.6	19.7	6.6	5.8	5.4	3.2	0.7	0.3	0.1	< 0.1	13.0
	< 2	< 2	< 10	< 5	< 5	< 10	< 20	< 15	< 25	< 20	
NaIdP	51.2	22.3	7.5	6.6	0.1	3.3	0.7	d.l	0.6	<0.1	8.0

	< 2	< 2	< 10	< 5	< 25	< 10	< 20	< 15	< 20

Trace metal compositions of the IdP and NaIdP samples are given in Supporting Information (Table S2). For both rocks, the order of concentrations is as follows: Rb, Ba, Zn (>150 $\mu g.g^{-1}$) > Cr, Cs (80-100 $\mu g.g^{-1}$) > Pb, As, La, Cu, Ga, Ni (50-20 $\mu g.g^{-1}$) > other TME including U (ca. 3$\mu g.g^{-1}$). It is to be noticed that concentrations are lower in NaIdP than in IdP for Sr (180 vs. 70 $\mu g.g^{-1}$), As and Ln, due to the removal of carbonate and/or phosphate minerals after rock conditioning.

3.2 Illite du Puy – solution interactions

Batch experiments were performed to gain insights into the evolution of the chemical composition of a solution in contact with Illite du Puy, for different clay-to-solution ratio ($R_{S/L}$). Supporting Information (Tables S3-4) shows values of pH, and concentrations of cations and anions (hereafter "$[]_{F,aq}$") of the final centrifuged solutions, for a 5-days contact with IdP. Experimental solutions at an initial pH of 2.29 ± 0.05 remain acidic for low $R_{S/L}$ (1-2 $g.L^{-1}$) and reach a near-neutral to slightly basic pH value for higher $R_{S/L}$ (3-6 $g.L^{-1}$). The slight and sharp increase of pH during experiments was likely due to fast reactions of protonation of functional groups existing at IdP surface (hydroxyl groups) and/or to mineral dissolution. Final concentrations of cations are in the order: $[Ca]_{F,aq}$ (1-2.5 mM) > $[K]_{F,aq}$ (230-300 µM) > $[Mg]_{F,aq}$ (50-120 µM). Silica concentration increases with final pH ($[Si]_{F,aq}$: 140-230 µM) whereas Al concentration sharply decreases ($[Al]_{F,aq}$: 110-10 µM). Major anions are fluoride ions and phosphate ions, which reach an almost constant concentration for a range of $R_{S/L}$ studied ($[PO_4^{3-}]_{F,aq}$: ~ 40 µM for $R_{S/L} \geq 2 g.L^{-1}$, Fig. 1), while sulfates and nitrates show much lower concentration values (<10 µM). Concentrations of uranium, nickel and lanthanides remain in the ppb level. Results of speciation calculations, performed by using the Visual MINTEQ (Ver 3.1) code and associated database, are reported in Supporting Information (Tables S5-6).

Phosphate ions are expected to be major ligands that influence the speciation of trace metals in the pH range 4–7, as well as carbonate ions for pH > 6.8, for solutions at equilibrium with atmospheric CO_2. Calculations also indicate that solutions at near-neutral pH ($R_{S/L} > 2$ g.L^{-1}) are oversaturated with respect to secondary phosphate minerals such as $AlPO_4 \cdot 1.5H_2O_{(S)}$, $MnHPO_{4(S)}$, and aluminum- or iron(III) - (oxihydr)oxides, which suggests that precipitation of secondary phases may possibly affect metal behavior in IdP-solution systems. An interesting feature is that, whatever the pH and $R_{S/L}$ values, $[Fe]_{F,aq}$ displays an almost constant value (ca. 3 μM) in the final solutions. Two tests of ultrafiltration at 3kDa of the centrifuged experimental solutions (at near-neutral pH) were made, which showed that the value of $[Fe]_{F,aq}$ decreased with an increase of the filtration threshold (Fig. 1). This evidences the formation of Fe-containing colloidal phases. Experimental results for NaIdP-solution systems are given in Supporting Information (Tables S3-4 and Figs. S3-4). It was observed that the Illite sample conditioning drastically decreased the values of $[Ca]_{F,aq}$ and $[anions]_{F,aq}$ of final experimental solutions, including for phosphate ions (Table S3). In contrast, $[Fe]_{F,aq}$ values remain of the same order of magnitude and the formation of colloidal phases containing Fe is likely regardless of the sample studied. For the NaIdP - solution systems, values of $[Si]_{F,aq}$ and $[Al]_{F,aq}$ sharply decrease with pH, suggesting a control by dissolution and/or precipitation of a same mineral phase, such as a clay. All these data support that macroscopic and spectroscopic work are needed to elucidate the speciation of phosphate ions on the clay surface, as they are major ligands of IdP-solution systems and can therefore strongly affect the sorption behavior of trace metals onto Illite du Puy.

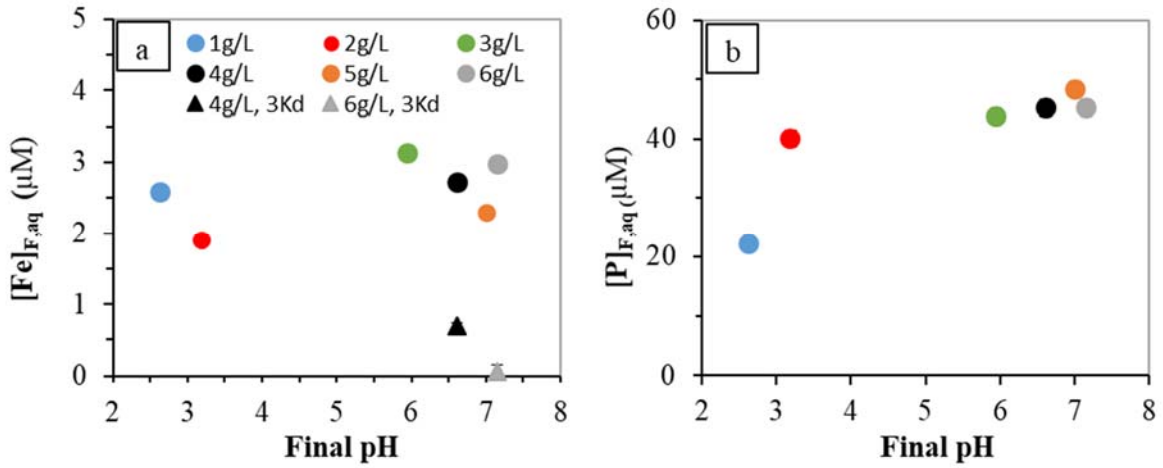

Fig. 1. Final experimental concentrations of (a) Fe ions and (b) phosphate ions vs. final pH of solutions contacted with Illite du Puy (IdP) at various IdP - solution ratios ($R_{S/L}$:1-6 $g.L^{-1}$). Experimental conditions: initial pH equal to 2.3, 0.005 M NaCl electrolyte, 5 days contact time. Circle and triangle symbols stand for solutions centrifuged and filtered at 3 kDa, respectively.

3.3 Macroscopic sorption behavior of phosphate ions

3.3.1 Sorption edge of phosphate ions

Fig. 2 shows a plot of the sorption edges of phosphate ions in NaIdP - 0.005 M NaCl electrolyte solution, at different values of total phosphate concentration ($[P]_{I,aq}$: 20 µM and 100 µM) and clay-to-solution ratio ($R_{S/L}$ = 1, 2 and 3 $g.L^{-1}$). The percentage of P sorbed is quite constant in the pH range 3-6, within our experimental uncertainties, and it decreases for pH values higher than 6. Several hypotheses may account for this pH dependence. First, a progressive deprotonation of the amphoteric silanol sites present at clay surfaces is expected when increasing pH to values higher than 6, consistently with the pK_a constant values reported in literature (Table S7, Supporting Information). Second, a pH value of 6 coincides with the appearance of the aqueous species HPO_4^{2-}, whose relative contribution to aqueous phosphate speciation becomes equal to that of $H_2PO_4^-$ at pH ca. 7.1 (Fig. S1, Supporting Information). All these features contribute to an increasing of electrostatic repulsion between clay surface and

aqueous phosphate at near-neutral to neutral pH, which is unfavorable to phosphate adsorption [68]. Fig.2b shows that the pH-dependence of surface coverage of NaIdP by phosphate ions (in $\mu mol.g^{-1}$) does not depend on the clay-to-solution ratio, at low $[P]_{I,aq}$ (20 µM), under the experimental conditions investigated ($R_{S/L}$:1-3 $g.L^{-1}$). This suggests that similar sorption sites and/or sorption species are involved whatever the $R_{S/L}$ value. In contrast, an increasing of the $[P]_{I,aq}$ value (from 20 to 100 µM) results in a strong decrease of the percentage of P sorbed, throughout the pH range investigated. A concomitant (non-linear) increase of surface coverage, is observable, too, and it is more marked at acidic pH than at pH higher than 6. This illustrates the existence of different types of phosphate sorption species with increasing surface coverage of NaIdP by phosphate ions. Sposito [80] proposed a value of density of surface sites onto soil minerals of 1.25-2.5 $sites.nm^{-2}$ in their modeling study of phosphate adsorption onto a soil. A value of surface site density of 2.31 $sites.nm^{-2}$ was proposed by Davis and Kent [81] for sites at illite platelet edges. Bradbury and Baeyens [77] used a value of 80 $\mu mol.g^{-1}$ (which would correspond to ca. 0.4 $sites.nm^{-2}$) for surface site capacity of Illite du Puy platelet edges (40 $\mu mol.g^{-1}$ for aluminol sites and 40 $\mu mol.g^{-1}$ for silanol sites) in their modeling study of experimental data on the macroscopic sorption of TME. These authors also considered a small amount (ca. 2 $\mu mol.g^{-1}$ or 0.01 $sites.nm^{-2}$) of high affinity sites present at edge clay platelets in order to successfully fit the TME sorption isotherms. Based on the surface site density values of Bradbury and Baeyens [77], it can be inferred that the sorption edges of phosphate ions reported in the present study would reflect P retention mechanisms that involve mainly the high-affinity sites existing at NaIdP particle edges, where strong interactions with adsorbate can occur, and that low-affinity edge surface sites have a limited contribution. At the highest P surface coverage studied (for $[P]_{I,aq}$ = 100 µM), multiple surface sites and/or phosphate sorption species are likely to be involved in the retention of P onto NaIdP.

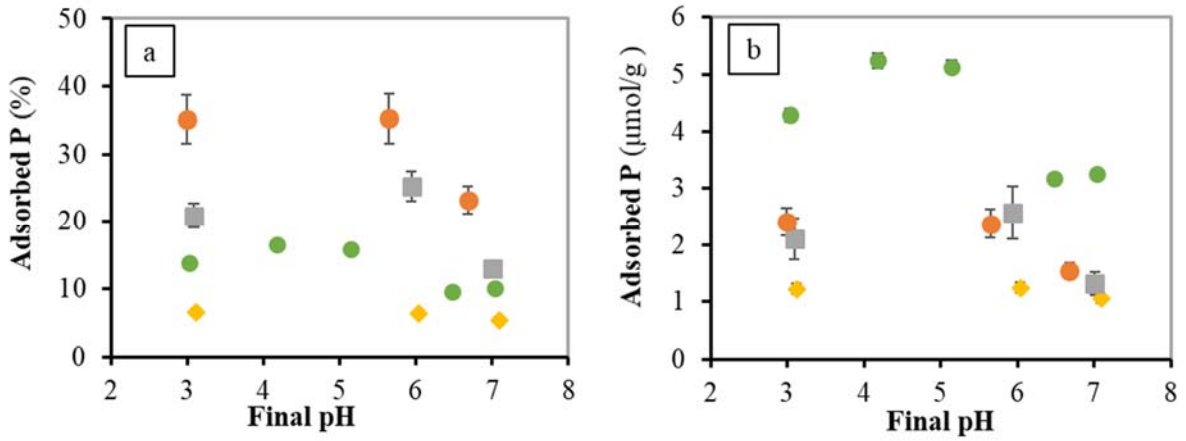

509

510 **Fig. 2:** Sorption edges of phosphate ions onto NaIdP: (a) percentage of P sorbed and (b) P
511 surface coverage (in µmol.g^{-1}) obtained at different clay-to-solution ratios, $R_{S/L}$ (♦: 1g.L^{-1}, ■:
512 2g.L^{-1} or ●●: 3g.L^{-1}), and total P concentrations, $[P]_{I,aq}$ (♦■●: 20µM or ●: 100µM).
513 Experimental conditions: 0.005 M NaCl electrolyte solutions, reaction time (t_R) of 4 days,
514 NaIdP-electrolyte solution system pre-equilibration (t_{pre-eq}) of 3 days.

515

516 3.3.2 Sorption isotherm of phosphate ions

517 Fig. 3 shows the sorption isotherm of phosphate ions onto NaIdP at acidic pH (pH_F: 4±0.05;
518 $[P]_{I,aq}$: 20-200 µM; $R_{S/L}$: 3 g.L^{-1}, t_{pre-eq}: 3 days, t_R: 4 days). At this pH value, main phosphate
519 species are $H_2PO_4^-$. There was observed a decrease in the percentage of P sorption with
520 increasing $[P]_{I,aq}$, which suggests the successive formation of several phosphate species at the
521 NaIdP–solution interface and/or a progressive saturation of different sorption sites present at
522 the clay edges. In contrast, surface coverage by phosphate (in µmol.g^{-1} clay, insert in Fig. 3)
523 increases when increasing $[P]_{I,aq}$ up to a value of ca. 50-60 µM. Such a behavior is typical of
524 the successive formation of various surface complexes of distinct stability and / or successive
525 implications of high-affinity and low-affinity surface sites for phosphate surface species
526 formation. A plateau in amount of phosphate ions sorbed (at 5-6 µmol.g^{-1} of phosphate sorbed)
527 is observable in Fig. 3 (insert) at $[P]_{I,\,aq}$ values higher than ≈ 60 µM. This result suggests a

saturation of all sorption sites available for phosphate retention. It also indicates no significant involvement of secondary processes like (surface) precipitation of phosphate phases, under the conditions investigated.

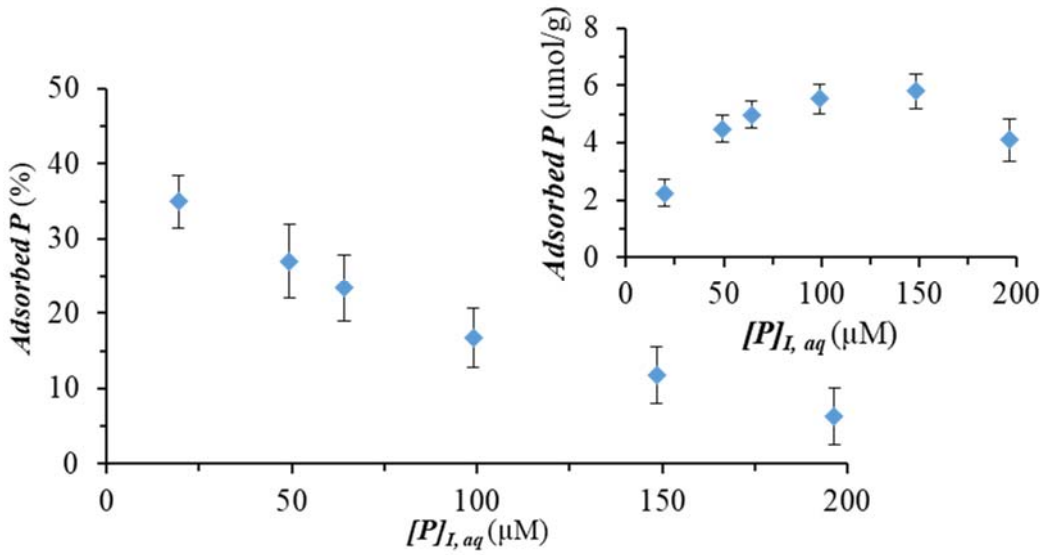

Fig. 3. Sorption isotherms of phosphate ions in % of adsorbed P (insert: P surface coverage in µmol.g^{-1}) onto NaIdP, at pH 4 and at $[P]_{I,aq}$ values in the 20-200 µM range. Experimental conditions: 0.005 M NaCl electrolyte solutions, $R_{S/L}$ = 3 g.L^{-1}, t_R = 4 days, $t_{pre\text{-}eq}$ = 3 days.

3.3.3 Electrophoretic mobility

Fig. 4 shows the pH dependence of electrophoretic mobility (EM) measured for NaIdP-0.005 M NaCl electrolyte suspensions at different $[P]_{I,aq}$ values. In the absence of any potential-determining ion other than OH^-/H^+, NaIdP particles display a low value of isoelectric point (IEP ≈ 3), *i.e.*, of pH at which EM and surface potential are equal to zero. This is consistent with previous studies reporting a low value of isoelectric point (IEP) for illitic minerals [82,83]. A sharp decrease of EM with pH is also observable in Fig. 4. These EM results reflect successive (de)protonations with pH of amphoteric surface functional groups (like silanol then aluminol / ferrinol sites) present on clay edge surface in NaIdP (cf. Table S7 in Supporting Information

546 for values of 1st and 2nd protonation constants of surface hydroxyl groups onto clay minerals).
547 Fig. 4 also reveals that, at acidic pH, EM of NaIdP in the suspensions is slightly diminished at
548 high phosphate concentration ($[P]_{I,aq}$ = 100 µM). This feature evidences a mechanism of
549 sorption of phosphate ions that adds negative charges to the clay surface.

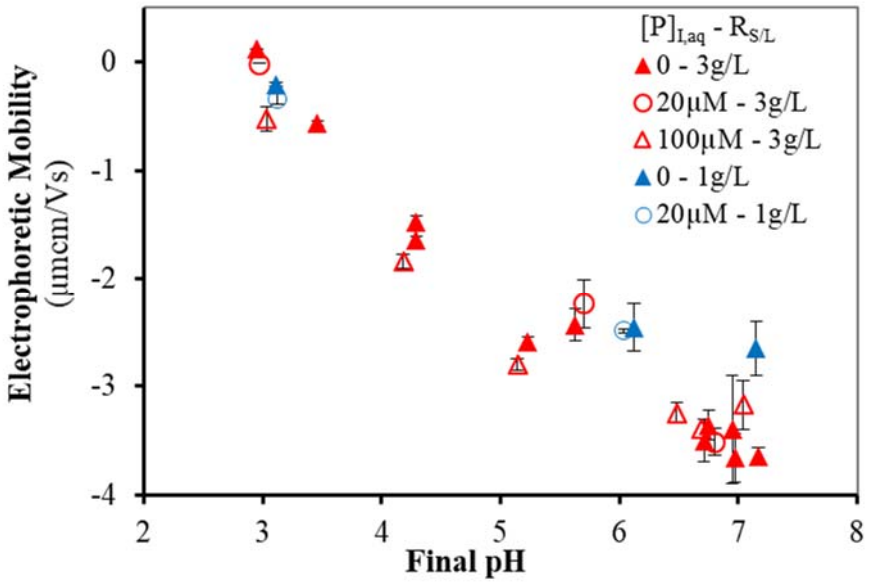

550

551 **Fig. 4**. pH dependence of electrophoretic mobility of NaIdP particles for experiments at
552 different initial concentrations of P ($[P]_{I,aq}$) and illite-to-solution ratios ($R_{S/L}$). Corresponding
553 data on P sorption are in Fig. 2. Experimental conditions: 0.005 M NaCl electrolyte solutions,
554 t_R = 4 days and t_{pre-eq} = 3 days for P sorption and t_R = 7 days for the experiments without P.

555

556 *3.4 ATR FTIR studies*

557 3.4.1 IR data on the clay structure or interface

558 ATR FTIR experiments were performed with the aim to identify positions of vibration bands
559 of the clay structure and / or clay-solution interface, *e.g.*, Si-O and/or Si-OH vibration bands,
560 which may interfere with ν(P-O) signals in the 900-1200 cm^{-1} range. In order to record a
561 significant IR signal, we followed the time evolution of the interface between illite and a not

562 equilibrated solution (cf. § 2.4.1 / 2.4.2). In these experiments, a thin layer of IdP or NaIdP was
563 coated on the ATR crystal surface and brought in contact with a 0.005 M NaCl solution at initial
564 pH 4 (no step of clay-solution pre-equilibration was made). Fig. 5a shows the evolution of in
565 situ IR spectra collected at the IdP–solution interface as a function of time. There was observed
566 since the first hour of IdP-solution contact the appearance in the spectral region 800-1200 cm^{-1}
567 of a strong "negative" absorbance whose growing rate decreases with time. Decomposition of
568 the spectra provided values of six vibration band maxima at 835, 873, 912, 979, 1040 and 1110
569 cm^{-1}. Table S8 in Supporting Information provides a succinct literature data on the OH
570 deformation and SiO stretching vibrational bands of clay minerals. The bands at 835, 873 and
571 912 cm^{-1} can be attributed to OH bending vibrational mode of Al-Mg-OH, Al-Fe-OH and Al-
572 Al-OH, respectively, in the structure of clay minerals [84,85]. The band at 979 [84], 1040 and
573 1110 cm^{-1} correspond to SiO stretching vibrational mode [84,86,87]. The main band at 980 cm^{-1}
574 is reported to be characteristics for Si-O stretching vibration of Si-O-H groups which is
575 attributed to asymmetric vibration of Si-OH, and it may reflect the presence of OH groups at
576 surface of polymerized silica [87]. Fig. 5b shows the time evolution of in situ IR spectra
577 collected at the NaIdP–solution interface. There was observed in the range 800-1200 cm^{-1} the
578 appearance of a low "negative" absorbance (which almost stabilizes after ca. 3 hours), showing
579 upon spectra decomposition three band maxima at 917, 966, and 1008 cm^{-1} as a main band. The
580 latter is characteristics of the Si-O stretching band in the micas group, like illite [88]. Hence,
581 the "negative" absorbance provides evidence for processes of structural reorganizations at the
582 illite-solution interface with time and / or clay dissolution during interaction of (Na)IdP and a
583 not equilibrated solution. In contrast, IR spectra recorded during ATR FTIR monitoring of the
584 interface between NaIdP and a nearly equilibrated solution (cf. § 2.4.1 / 2.4.3) showed, and
585 only after a reaction time of 3 days, a very low absorbance that was found to be insignificant

compared with that observable in the interface FTIR spectra of sorbed phosphate species (cf. § 3.4.3).

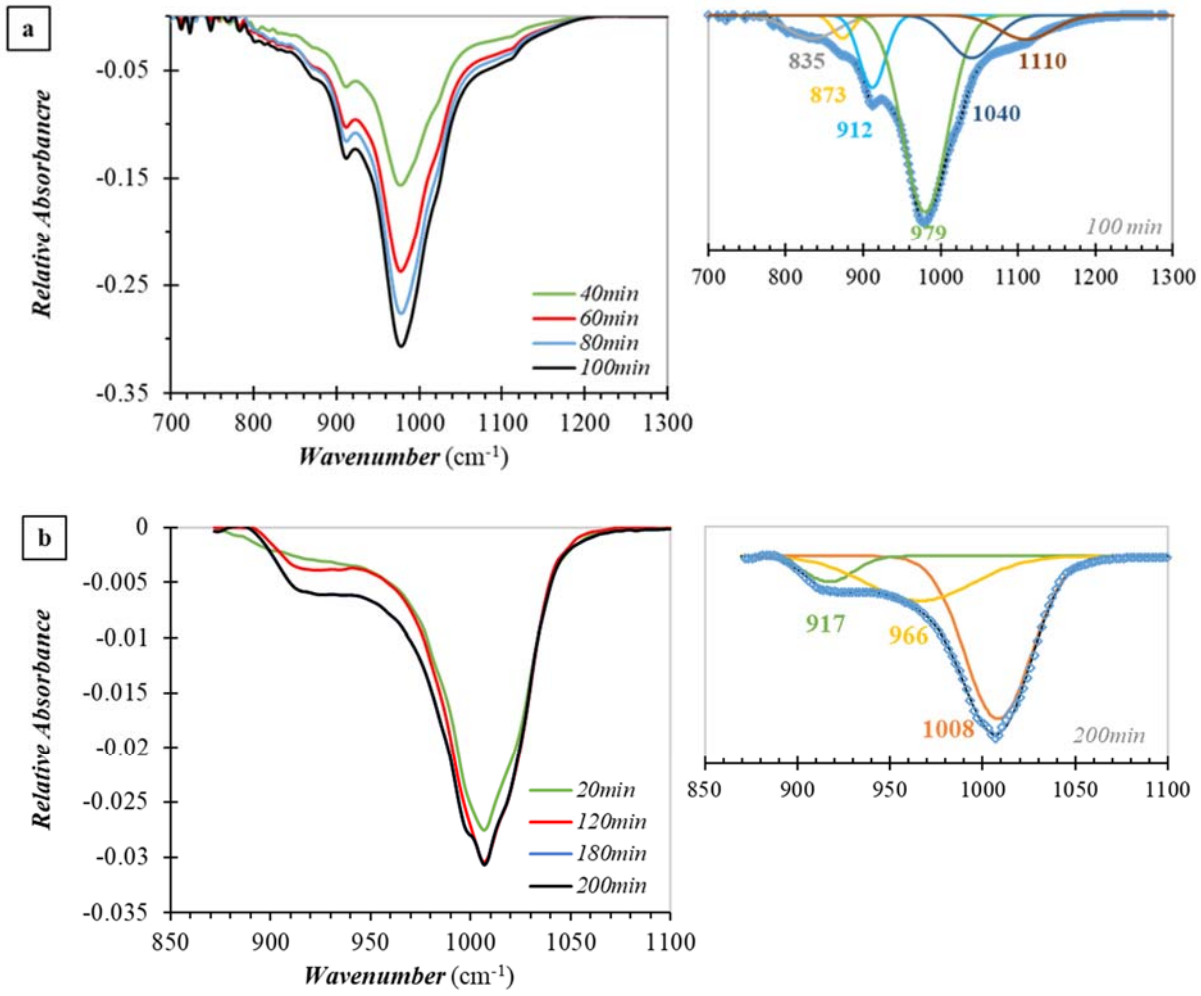

Fig. 5. Time evolution of in situ ATR FTIR interface spectra recorded along interaction of (a) IdP or (b) NaIdP in contact with a (not pre-equilibrated) 0.005 M NaCl electrolyte, at an initial pH of 4 (final pH: 6.2 and 4.0, respectively) and results of spectra decomposition (insert). The solutions were added to a thin film of clay coated on the ATR crystal (cf. § 2.4.1 / 2.4.2).

3.4.2 IR spectra of aqueous solutions containing PO_4^{3-} and Fe^{3+} ions

IR spectra of 0.005M NaCl electrolyte containing P(V) at different concentrations ($[P]_{I,aq}$: 20-225µM) in the pH range 4-7 are presented and commented in Supporting Information (cf. Fig. S2 and §2). The υ_3(P-O) bands at 1160 and 1075 cm^{-1} of $H_2PO_4^-$ were observable at pH 4 and the detection limit for this aqueous species was estimated to be approximately of 45 µM, a

599 concentration at which IR band intensities are very close to background noise level. Although
600 the concentration of Fe^{3+} ions released in aqueous solution was found to be low (<4µM) in our
601 experiments of (Na)IdP-solution interactions (cf. §3.2), ATR FTIR analyses were made to
602 determine the IR band positions of aqueous iron(III)–phosphate species. The analysis was
603 expected to be helpful to detect the potential contribution of OSSC and ISSC of iron–phosphate
604 species to IR signals of the NaIdP-phosphate-solution interface. Fig. 6a compares IR spectra of
605 solutions at pH 4 containing phosphate ions ($[P]_{I,aq}$ of ca. 100µM), in the absence and in the
606 presence of Fe(III). Note that the absorbance observable in the IR spectrum recorded for the
607 solution containing P(V) only is weak, although the IR bands at 1160 and 1075 cm^{-1}
608 characteristics of the diprotonated phosphate ion $H_2PO_4^-$ are defined. It was found that, due to
609 formation of iron(III)-phosphate aqueous complexes, the addition of 10µM of Fe(III) in the
610 phosphate solution at pH 4 slightly increases the absorbance recorded in the wavenumber range
611 1000-1150 cm^{-1}, with a large main band being observable. Fig. 6b shows that four IR absorption
612 bands at 1041, 1085, 1124 and 1149 cm^{-1} were resolved upon decomposition of the IR spectra
613 of the aqueous solution containing Fe^{3+} and PO_4^{3-} ions, with an additional weak band at 1077
614 cm^{-1} attributable to $H_2PO_4^-$ almost disappearing with time (after ca. 2h) upon formation of the
615 iron(III)-phosphate complexes. Based on the FTIR data given by Tejedor-Tejedor and
616 Anderson [3], the bands at 1041, 1089 and 1149 cm^{-1} could be attributed to $FeHPO_4^+$ aqueous
617 complex, the main species dominating the speciation of Fe under the conditions investigated
618 (and to additional contribution of $FeH_2PO_4^{2+}$, a minor species). The bands at 1043 and 1125
619 cm^{-1} could relate to the $Fe_2PO_4^{3+}$ species [3]. $Fe_2(OH)PO_3^{2+}$ aqueous species is reported to
620 display a set of bands at 1041,1085 and 1124 cm^{-1} but it is not significantly formed at pH 4.

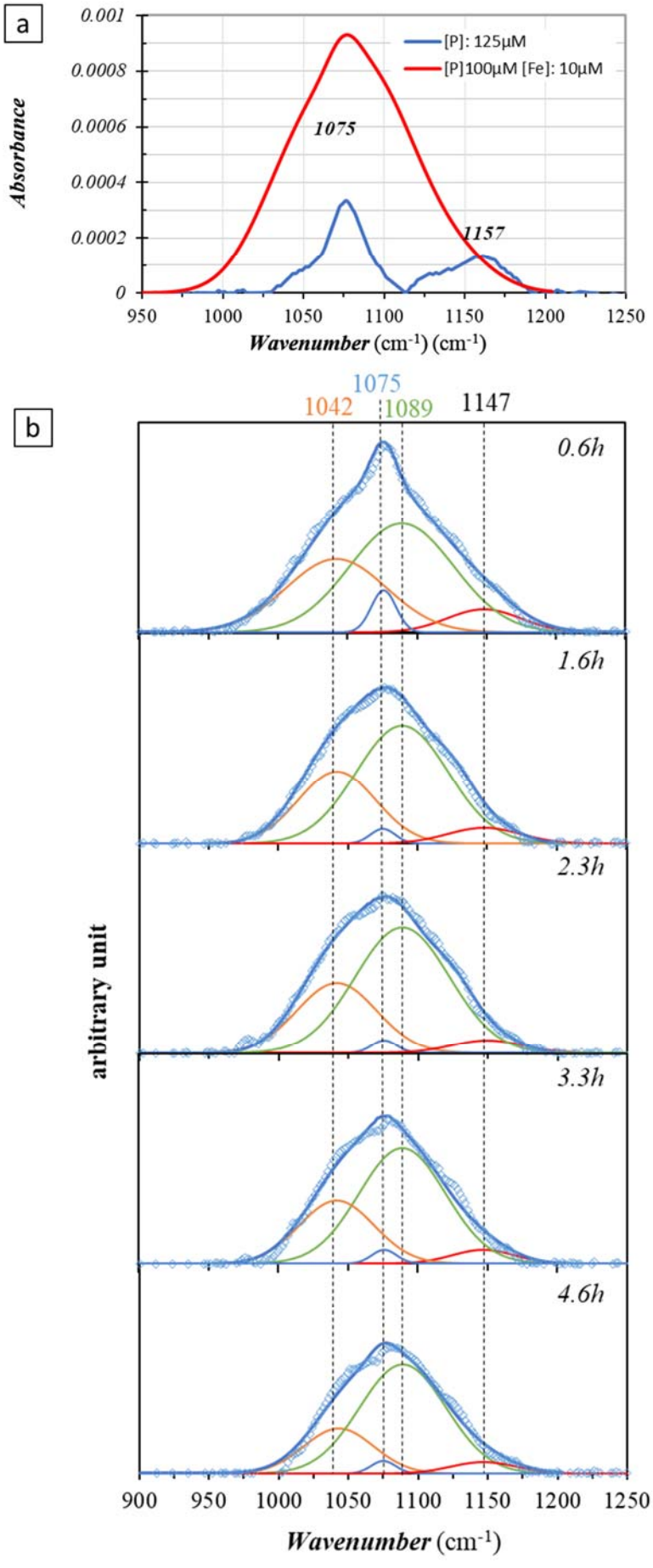
a
0.001
0.0008
0.0006
0.0004
0.0002
0
Absorbance
[P]: 125μM
[P]100μM [Fe]: 10μM
1075
1157
950
1000
1050
1100
1150
1200
1250
Wavenumber (cm-1) (cm-1)
b
1075
1042
1089
1147
0.6h
1.6h
2.3h
3.3h
4.6h
arbitrary unit
900
950
1000
1050
1100
1150
1200
1250
Wavenumber (cm-1)

621

622 **Fig. 6.** ATR FTIR spectra of 0.005 M NaCl electrolyte solutions at pH 4: (a) effect of presence
623 of Fe(III) ($[Fe]_{I,aq}$: 10µM) in a phosphate solution ($[P]_{I,aq}$: 100 or 125µM, t_R: 4.6 hours) and (b)
624 effect of reaction time on a solution containing Fe(III) and P(V) ions ($[P]_{I,aq}$:100 µM, $[Fe]_{I,aq}$:
625 10 µM). Circles: experimental curve; lines: results of spectrum decomposition.

626

627 3.4.3 ATR FTIR monitoring of phosphate sorption at clay – solution interface

628 It should be pointed out that in the ATR FTIR phosphate sorption experiments presented below
629 (IR spectra reported in Figs. 7 and 8), phosphate sorption monitoring was carried out at the
630 interface between NaIdP and a nearly equilibrated electrolyte solution, that is to say, between a
631 layer of NaIdP particles that had previously been allowed to settle on the ATR crystal for 3 days
632 from a NaIdP-solution suspension at pH 4. The suspension was itself pre-equilibrated for 3 days
633 before being added to the ATR cell (cf. §2.4.1 and §2.4.4). The NaIdP-solution bilayer system
634 studied by ATR FTIR spectroscopy was therefore almost at equilibrium before the start of the
635 phosphate sorption experiment, in order to minimize clay dissolution and structural
636 reorganization and/or the formation of surface hydroxyl groups on the clay during the phosphate
637 sorption process. In addition, blank ATR FTIR monitoring experiments of the NaIdP-solution
638 bilayer system at pH 4 (cf. §2.4.3) provided interface IR spectra showing only a very weak IR
639 signal in the 900-1200cm^{-1} wavenumber range, which proved negligible compared with those
640 obtained in the presence of phosphate ions, whether short, intermediate (Fig. 8a) or long
641 reaction times (Fig. S5 in Supporting Information) are considered.

642 *Effect of reaction time*. Fig.7a shows the ATR FTIR spectra recorded by in situ monitoring of
643 the sorption of phosphate ions at NaIdP–solution interface at pH 4 (two successive additions,
644 at t_R = 0 and 1 hour, respectively, of 50µM of aqueous P to a nearly equilibrated NaIdP–solution
645 bilayer system, cf. §2.4.1 and 2.4.4). There was observed the appearance of a weak absorbance
646 in the whole region 1050-1250 cm^{-1} after addition of 50 µM of P, which slightly increases with

an increasing of total phosphate concentration to a value of 100 µM (cf. spectra at $[P]_{I,aq}$ = 50µM / t_R = 20min and $[P]_{I,aq}$ = 100 µM / t_R = 1h20min, respectively). From short to intermediate reaction times (t_R of ca. 19h), there was observed the appearance and the progressive increase of a broad absorbance at lower wavenumbers, which increases dramatically up to a reaction time of 3 days and shifts the IR absorption signals towards the region 1000-1100 cm^{-1}.

At short reaction time (t_R < 8 hours), the absorbance observed on the IR spectra of the interface is weak, which makes it somewhat difficult to decompose the signals. However, it can be inferred from spectra decomposition (Fig. 7b) that the very short-term spectra (t_R < 1h20min) were dominated by two broad bands centered at 1075 and 1160 cm^{-1}, with a small shoulder centered at 1035 cm^{-1}. Peak maxima position of the two broad bands were similar to those recorded for the phosphate–solution system under similar conditions (Fig.S2 in Supporting Information) but their intensity is higher. This suggests that at least a fraction of aqueous phosphate ions was involved in the formation of a phosphate surface species onto NaIdP (hereafter "species A"). Decomposition of spectra reveals that the intensity of the two bands of species A show a progressive decrease with time (for t_R > 2 hours), until disappearance (Fig. 7b). In contrast, a band centered at 1035cm^{-1} (which occurred as a broad shoulder on the short-term spectra) increases slightly with time (t_R < 8h). A poorly-defined band centered at ca. 1132 cm^{-1} could be also identified. It seems that the latter band is independent of the concentration of phosphate ion and reaction time. At an intermediate reaction time (t_R = 19h), the band positioned at 1035 cm^{-1} is well resolved and its intensity shows a further dramatic increase with time (t_R = 3 days). A shoulder at a lower wavenumber (at 1003 cm^{-1}) and a band positioned at 1095cm^{-1} are also present in the IR interface spectra collected at intermediate and long reaction times. We assign the bands at 1003, 1035, 1095 and 1132 cm^{-1} to υ_3 (P-O), as the IR active υ_1 (P-OM, M: metal or hydrogen atom) bands are located at wavenumbers lower than 900 cm^{-1} [7]. The maxima positions of the three υ_3 (P-O) bands are different from those of aqueous

672 $H_2PO_4^-$ species and phosphate surface species A, which evidences that at least another
673 phosphate surface species is formed at the interface. These positions differ also significantly
674 from those observable for the vibration bands of $FeHPO_4^+$ aqueous complex (bands at 1041,
675 1089 and 1149 cm^{-1}), which is the main species expected to dominate the aqueous speciation
676 of Fe(III) under the conditions investigated (cf. §3.4.2). It must also be pointed out that a
677 contribution to the IR spectra (Fig. 7) from an IR signal originating from the structural
678 reorganization over time of surface hydroxyl groups and / or clay is to be excluded at $t_R < 19h$
679 (Fig. 8a) and is very weak at a long reaction time of 3 days (Fig. S5 in Supporting Information),
680 as "blank" FTIR spectra of the clay-solution interface recorded in the absence of phosphate ions
681 showed only low absorbance (Fig. S5). Hence, based on band maxima positions observable
682 from short to long reaction times in the FTIR spectra of the NaIdP-phosphate-solution interface
683 in Fig. 7, we interpret the evolution of the IR signals by the formation of a P surface species
684 (hereafter "species B") whose contribution grows with time. Further addition of phosphate ions
685 (100 µM) to the 3-days aged system induced no significant change in band's intensity, which
686 rather suggests that no additional surface complex and / or precipitate of phosphate is formed
687 onto NaIdP under the investigated conditions, in good agreement with the results of the
688 macroscopic sorption experiments (cf. § 3.3.2). The increase of absorbance of the band at 1035
689 cm^{-1} and the decrease of that at 1075 cm^{-1} with time may reflect the kinetics of a conversion
690 from outer sphere (species A) to inner sphere (species B) surface complex of phosphate.

691

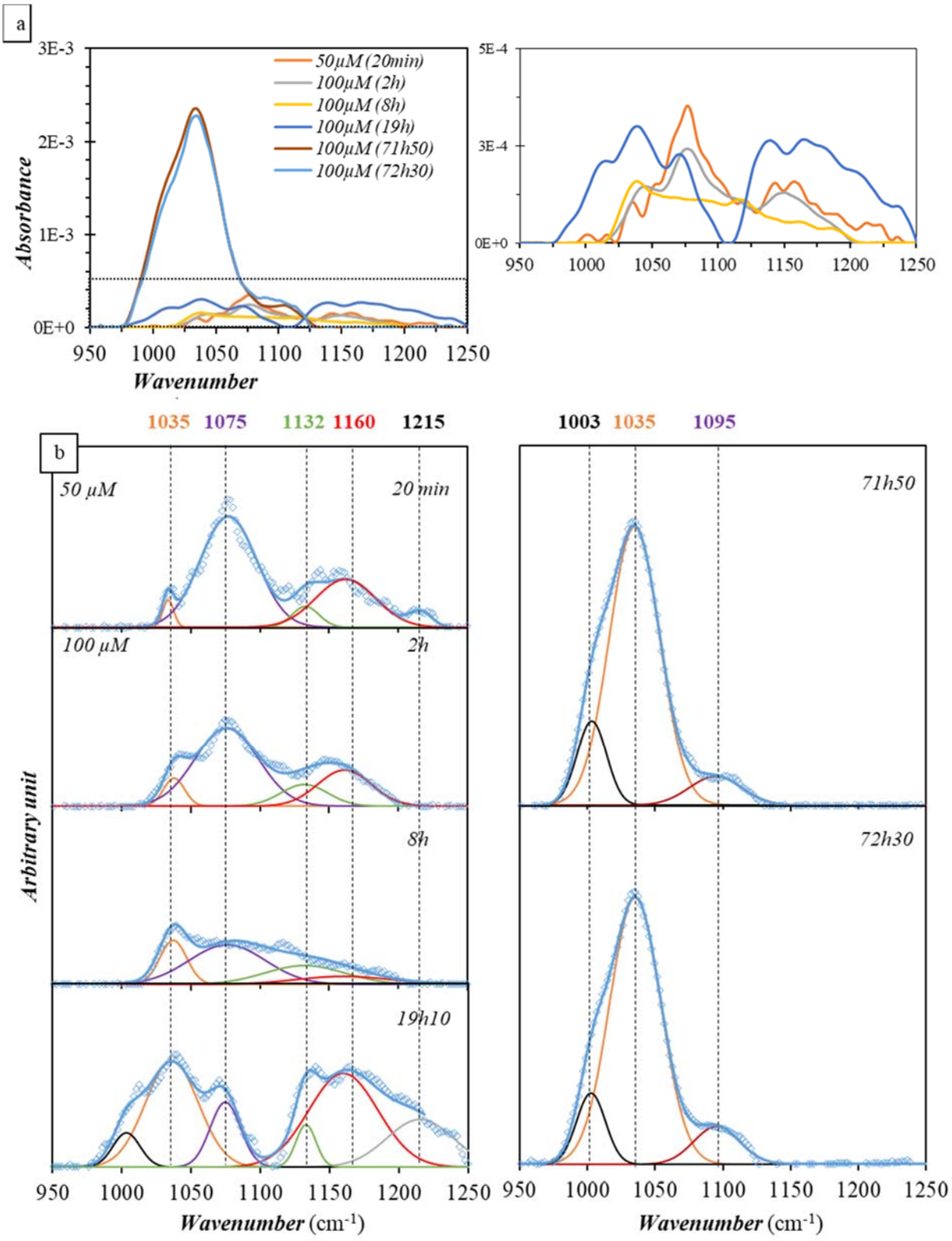

Fig. 7. (a) Evolution of in situ ATR FTIR spectra recorded at the NaIdP – phosphate - solution interface as a function of time, and (b) results of spectra decomposition. Experimental conditions: 0.005 M NaCl electrolyte solution at pH 4, $[P]_{I,aq}$ of 50 µM (20min), 100 µM (t_R: 2

hours up to 3 days). Aqueous phosphate was added to a nearly equilibrated NaIdP – solution bilayer system deposited on the ATR crystal (cf. §2.4.1 and §2.4.4).

Effect of phosphate ion concentration - Fig. 8 shows the ATR FTIR spectra recorded by in situ monitoring of phosphate ion sorption at the NaIdP–solution interface, as a function of the total phosphate concentration ($[P]_{I,aq}$: 50-300 µM), at pH 4 and at a reaction time < 24 hours (successive additions of aqueous P to a nearly equilibrated NaIdP–solution bilayer system, cf. §2.4.1 and §2.4.4). There was observed an increase of IR absorbance with increasing phosphate concentration (Fig 8a). At low phosphate concentration (50 µM), a well-defined band at 1075 cm^{-1} and a broad band were present in the 1000-1250 cm^{-1} wavenumber region. Results of spectra decomposition (Fig. 8b) indicate that the broad band maximum is located at 1160 cm^{-1}, with two shoulders at 1215 cm^{-1} and at 1132 cm^{-1}. These bands (i.e., 1075, 1132, 1160 and 1215 cm^{-1}) are present in the range of phosphate concentration 50-250 µM. At a $[P]_{I,aq}$ value of 100 µM and an intermediate reaction time (t_R=2 hours, Fig. 8a), a shoulder of weak absorbance appears at a wavenumber lower than that of the band at 1075 cm^{-1}. This evolution is similar to that reported in the previously-described ATR FTIR phosphate sorption experiment (cf. Fig. 7). An increasing of absorbance was observable with increasing total concentration of phosphate, which appeared to be due to the growing of a well-defined P-O stretching band with a maxima at 1035 cm^{-1} (Fig. 8b). At $[P]_{I,aq}$ values higher than 150 µM, another small shoulder centered at 1005 cm^{-1} appeared and increased with increasing phosphate concentration. These bands are similar to those identified for the phosphate surface species B in the previously-described ATR FTIR experiment. The band at 1095 cm^{-1} (of species B) could not be observed at $[P]_{I,aq}$ < 250 µM, possibly due to overlapping of the band at 1075 cm^{-1} which exhibited a strong absorbance. Note that a significant contribution of IR signals originating from the structural reorganizations of surface hydroxyl groups or clay appear unlikely, given the negligible absorbance observable

720 in “blank” IR spectra (Fig. 8a) recorded after 20h of ATR FTIR monitoring of the nearly
721 equilibrated NaIdP – solution bilayer system without P (blank experiment, cf. §2.4.3).

722 Hence, seven absorption bands (at 1003, 1037, 1075, 1095, 1132, 1160 and 1215cm^{-1}) were
723 identified on the FTIR NaIdP-phosphate–solution interface spectra recorded when the
724 concentration of phosphate ion is increased in experiment. These bands are assigned to the same
725 surface species as those identified in the previously described ATR FTIR phosphate sorption
726 experiment on the effect of reaction time. The bands at 1075, 1160 and 1215 cm^{-1} correspond
727 to the species A. The bands at 1003, 1037, 1095 -and possibly 1132 cm^{-1}- relate to the species
728 B. Note that the band at 1132 cm^{-1} of low absorbance is independent on phosphate concentration
729 ($[P]_{I,aq} < 250$ μM) and reaction time (for $t_R < 19$ hours).

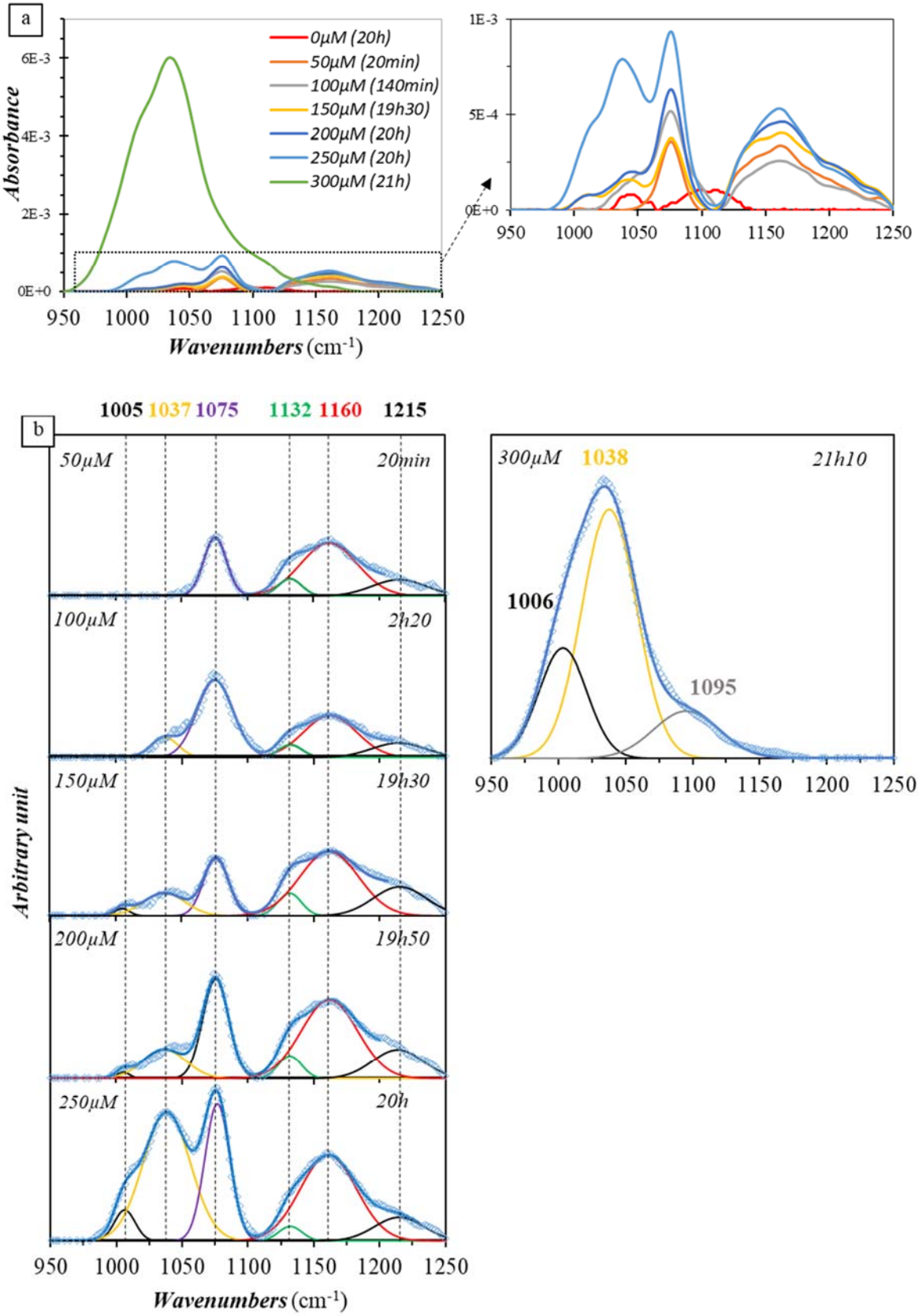

730

731 **Fig. 8**. (a) Evolution of in situ ATR FTIR spectra recorded at the NaIdP–solution interface

732 along an increase of P concentration in experiment ($[P]_{I,aq}$: 50-300 µM) and (b) results of

733 spectra decomposition. Experimental conditions: 0.005 M NaCl electrolyte solution at pH 4, t_R
734 up to 21 hours. Successive additions of P (§2.4.4) were made to a nearly equilibrated solution-
735 clay bilayer system deposited on the ATR crystal (cf. §2.4.1). In situ ATR FTIR spectrum
736 recorded after 20h of monitoring of the solution-clay bilayer system without P (blank
737 experiment, cf. §2.4.3) is also given in (a).

738 **4 Discussion**

739 *4.1 Macroscopic sorption of phosphate ions at illite–electrolyte solution interface*

740 Sorption edges of phosphate ion sorption onto NaIdP presented here for low $[P]_{I,aq}$ values (<
741 100 μM) show that the highest percentage of phosphate sorption was found at acidic pH (3-6),
742 with this percentage decreasing with increasing pH. This findings are consistent with previous
743 studies of phosphate ion sorption onto aluminum-oxide, illite, and kaolinite [8,13,22]. Del Nero
744 et al. [8] showed a maximal and quite constant sorption of phosphate ions onto alumina at pH
745 3-6, and a decrease in sorption at higher pH. The authors proposed that two sorption
746 mechanisms, i.e., formation of ISSC/OSSC and surface precipitation of Al-phosphates, were
747 involved in the retention of phosphate ion at the alumina-electrolyte solution interface when P
748 loading increases at acidic pH. At low surface coverage, P sorption was shown to be controlled
749 by reactions of surface complexation *i.e.*, by surface ligand exchange reactions implying high
750 affinity aluminol edge sites, and by formation of an outer-sphere phosphate surface complex at
751 protonated aluminol surface sites (e.g., $\equiv AlOH_2^+$). Edzwald et al. [22] examined the
752 macroscopic uptake of P by (not conditioned) clay minerals like illite, kaolinite and
753 montmorillonite. They observed that the sorption of phosphate ions was maximal at pH 4-5 and
754 further decreased at higher pH, which is a similar pH-dependence than that observed in the
755 present study for NaIdP. The authors concluded that the aluminol surface groups of clays, which
756 have an isoelectric point at high pH, are more important in sorption of phosphate ions than the
757 silanol surface groups (which have a negative charge down to a pH of 2). Edzwald et al. [22]

also emphasized that the adsorbed metals (e.g., iron) as bridging cations present at the surface of clay and/or the metal (e.g., Fe- and Al-) oxides contained in the clay sample, controls the retention of phosphate ions. Van Emmerik et al. [13] studied the sorption of phosphate ions onto a pretreated kaolinite (at concentrations of phosphate ions in the range 1-10 mM). Their data also showed that the percentage of phosphate ion sorption was maximal and constant in the range of pH 3-5 and decreased with pH, at low and high surface loadings. They reported that formation of ISSC and/or surface precipitates of phosphate at edge sites of the alumina-like layer of kaolinite was predominant over the studied pH range, depending on surface loading by phosphate ions. The sorption edge and sorption isotherms of phosphate ions on NaIdP presented in the present study are consistent with the above-mentioned studies, which suggest a predominant role on P sorption of the aluminol and/or ferrinol surface sites present at edges of illite. Our macroscopic data suggested the successive formation, with increasing $[P]_{I,aq}$ (< 200 µM) or with decreasing $R_{S/L,}$ of surface complexes of distinct stability. Alternately, high-affinity and low-affinity surface sites might be successively implicated in formation of phosphate surface species onto NaIdP, up to a surface coverage of ca. 5-6 $\mu mol.g^{-1}$ for which no clay surface sites are available anymore for P sorption (see § 3.3.1, §3.3.2). Such a limiting surface coverage is consistent with values of surface concentrations of low affinity and high affinity aluminol sites expected to exist at NaIdP clay platelets [77]. It is unlikely that significant amounts of Al-phosphate surface precipitates are involved in phosphate ion sorption onto NaIdP under our experimental conditions ($[P]_{I,aq} \leq 200\mu M$), as P surface coverage reaches a plateau. Therefore, the aluminol surface sites at NaIdP edges mostly participate to the formation of ISSC of phosphate under our investigated conditions, which may be favored at acidic pH by a first step of electrostatic attraction between the positively charged clay surface (due to existence of protonated aluminol sites as ΞSOH_2^+ and the negatively charged aqueous phosphate ions (HPO_4^{2-} and $H_2PO_4^-$) approaching the surface (formation of OSSC of phosphate). EM

783 measurements are useful to determine the isoelectric point (IEP) of colloidal materials as well
784 as to distinguish ISSC from OSSC formation [6,89]. Later surface species are reported to
785 influence the value of EM but they do not produce changes in IEP, whereas ISSC formation
786 may lead to surface charge reversals and shifts in IEP [6,8,89]. EM data showing charge reversal
787 and IEP shifts to lower pH value with increasing phosphate loading onto minerals were reported
788 in the literature as indirect evidences of formation of ISSC of phosphate ions at the interface
789 between solution and kaolinite or iron / aluminum (hydro)oxides [3,6,8,10,15,90]. As long as
790 the edge aluminol (and/or ferrinol) sites are responsible for phosphate sorption onto clay,
791 sorption reactions of phosphate ions at such sites would play a role on surface charge evolution
792 of clay. The data presented here show a slight decrease in EM as a consequence of phosphate
793 ion sorption onto NaIdP at acidic pH, which suggests a mechanism of P sorption imparting
794 negative charges to the clay surface.

795 *4.2 ATR FTIR spectroscopic study of P sorption at illite–solution interface at pH 4*

796 *Phosphate surface species A (1075, 1160 and 1215 cm^{-1}).*

797 Phosphate surface species A has two υ_3 bands at 1075, 1160 cm^{-1} and a broad band centered at
798 1215 cm^{-1}. The position of these bands are very similar to those of the dissolved phosphate
799 species ($H_2PO_4^-$, C_{2v}), as reported by [3]. The latter also have a band at 1215 cm^{-1} assigned to
800 the δ(P-OH) bending mode of dissolved phosphate species (e.g., $H_2PO_4^-$, C_{2v}) [3,6,7,78]. In the
801 present study, a broad and weak band at 1215 cm^{-1} is present in IR interface spectra recorded
802 at short reaction time during the sorption process of phosphate ions at the interface (while it
803 was not observed in IR analyses of the phosphate – electrolyte solution system). That the band
804 at 1215 cm^{-1} of the δ(P-OH) bending mode was observed during the P sorption process
805 suggested the formation of OSSC species of phosphate. Accumulation of negatively charged
806 phosphate ions by electrostatic attraction as counter-ions to balance positively charged edge
807 sites created at the clay-solution interface, i.e., ΞSOH_2^+ sites, and/or by weak hydrogen bonding

to surface water or surface hydroxyl sites, might increase their absorbance. Molecular symmetry of sorbed phosphate ions is expected to be similar to that of dissolved phosphate species (C_{2v}) if the phosphate ions is weakly sorbed. The numbers of P-OH bands of the weakly sorbed phosphate should be the same as for the corresponding aqueous P species, and the peak position should be close, too [6]. The maximal number of υ_3 vibrational bands of PO_4 unit for a C_{2v} or lower molecular symmetry is three [7] because the υ_3 vibrational bands is triply degenerated when PO_4 units have a T_d molecular symmetry mode [91]. Theoretically, the third υ_3 band located at 940 cm^{-1} should be present in IR signals for an OSSC species of phosphate. The band was however not observable in our IR interface spectra possibly due to: (i) the strong IR absorbance of NaIdP–solution system below 1000 cm^{-1} as observed by Borgnino at al. [23] for an iron modified montmorillonite, and (ii) cutoff of detector at ~ 900 cm^{-1}. We thus conclude that the phosphate surface species A with IR bands at 1075, 1160 and 1215 cm^{-1} is an OSSC of diprotonated phosphate ions (as $\Xi SOH_2^+ \ldots H_2PO_4^-$) formed at NaIdP–solution interface, which predominates the phosphate surface speciation at short reactions times and / or at low P concentrations.

Phosphate surface species B (1005, 1037, 1095 and 1132 cm^{-1}).

Phosphate surface species B has four υ_3 bands at 1005, 1037, 1095 and 1132 cm^{-1} whose band intensity increases with reaction time -except the poorly-defined band at 1132 cm^{-1}. This species exhibits a vibration band at 1035 cm^{-1} that predominates at a long reaction time (> 24 hours). Borgnino et al. [23] have shown in an ATR FTIR study of phosphate sorption at the Fe-modified montmorillonite–solution interface that, at a low pH value, two ISSC of phosphate were formed at the surface of iron(III) (hydr)oxides present in the clay. The first one was shown to be an unprotonated bidentate surface complex $\Xi(FeO)_2PO_2$, with υ_3 bands at 1088, 1049 and 941 cm^{-1}. The authors suggested a C_{2v} or lower molecular symmetry for this ISSC, whose band maxima positions resulted from shifts of υ_3 bands of $H_2PO_4^-$ (at 1160, 1076 and 940 cm^{-1}). The second

one was proposed to be a monoprotonated bidentate surface complex, e.g. $\Xi(FeO)_2(OH)PO$, whose bands' positions were at 1128, 1011 and 978 cm^{-1}, with a C_1 molecular symmetry. Dolui et al. [19] investigated the mechanisms of phosphate sorption ($[P]_{I,aq}$ = 100 μM) at acidic pH at the kaolinite–solution interface by using in situ ATR FTIR spectroscopy and they identified five υ_3 bands (1138, 1108, 1086, 1074 and 1061 cm^{-1}). They reported the formation of multiple surface species of phosphate ions at the surface of kaolinite with a predominant surface species (ISSC or surface precipitate) formed at edge aluminol sites whose band position was at 1138 cm^{-1}. Li et al. [69] studied surface speciation of phosphate ions at the α-Al_2O_3–electrolyte solution interface from pH 5 to 9 by using ^{31}P solid state NMR coupled with ATR FTIR and DFT calculation. Five IR bands (at 1130-1131, 1092-1096, 1053-1060, 1020-1025 and 1005-1010 cm^{-1}) were identified. The authors concluded on the co-existence of two surface complexes of phosphate ions as predominating surface species at pH 5: a monoprotonated bidentate binuclear surface complex, as $\Xi(AlO)_2(OH)PO$ and an unprotonated bidentate binuclear surface complex, as $\Xi(AlO)_2PO_2$. The authors observed at high pH a decrease in intensity of bands at 1130 and 1010 cm^{-1}, which relate thus to the protonated species (and bands at 1096, 1060 and 1020 cm^{-1} may relate to unprotonated species). Del Nero et al. [8] investigated the sorption mechanisms of phosphate ions at acidic pH onto α-Al_2O_3 by in situ ATR FTIR spectroscopy and zeta potential measurements. They reported formation at low surface coverage of an ISSC of phosphate that decreased the surface charge of alumina and had possibly IR bands at 1084 and 1033 cm^{-1}. The main phosphate surface species was shown to become progressively a surface precipitate of Al-phosphate incorporating Al^{3+} ions released by mineral dissolution, with a band at 1137 cm^{-1} and a constant surface charge, when increasing surface coverage by phosphate ions. Based on bands' positions, molecular symmetry considerations, and above-mentioned literature data, we assign the three υ_3 bands positioned at 1005, 1037 and 1095 cm^{-1} for species B identified in the present study to a monodentate binuclear surface

858 complex species formed at edge surface sites (S) of clay, i.e., $\Xi(SO)_2PO_2$, likely via surface
859 ligand exchange implying high-affinity aluminol sites on the edge of illite platelets, and, to a
860 lesser extent, low-affinity aluminol surface sites. The symmetry of the phosphate unit for
861 species B is C_{2v} or lower. The small υ_3 bands at 1132 cm^{-1} can be tentatively assigned to limited
862 formation of a monoprotonated monodentate binuclear surface complex $\Xi(SO)_2(OH)PO_2$ as
863 similar band position were reported for ISSC of phosphate of the type $\Xi(SO)_2(OH)PO_2$ by Li et
864 al. [69] and $\Xi(FeO)_2(OH)PO_2$ by Borgnino et al. [23]) formed onto Al- and Fe-oxides,
865 respectively, and / or to low amounts of Al-phosphate surface precipitates.

866 **5 Conclusions**

867 This study provides new insights into the sorption mechanisms of phosphate ions at the illite –
868 solution interface, for a range of aqueous phosphate concentrations (20-200 µM) and clay-to-
869 solution ratios that led to low to moderate coverage of the clay surface by P (2-6 $\mu mol.g^{-1}$). It
870 was found that the percentage of P sorption is dependent on pH and the coverage of the clay
871 surface by phosphate. At high P loading, the process of phosphate sorption added negative
872 charges to the clay surface and involved multiple sorption species and/or surface sites present
873 on the clay edges. Data acquired by in situ monitoring of the illite-solution interface by ATR
874 FTIR spectroscopy provided evidence that phosphate ions were primarily sorbed at acidic pH
875 via the increasing formation, with time and aqueous phosphate concentration, of inner-sphere
876 phosphate surface complexes, probably monodentate binuclear surface complexes, i.e.,
877 $\Xi SO)_2PO_2$, through surface ligand exchange involving hydroxyl surface sorption sites (S) on
878 the clay edges, likely the high affinity aluminol sites and, to a lesser extent, low affinity
879 aluminol sites. These surface species were characterized by υ_{as}(P-O) bands positioned at 1003,
880 1035 and 1095 cm^{-1}, and were formed by transformation over time of an outer-sphere phosphate
881 surface complex that dominates phosphate surface speciation at low reaction times and low P
882 concentration. The information on phosphate surface speciation presented here is novel, and

provides for the first time in situ spectroscopic evidence of strong sorption of phosphate ions at the surface of a 2:1 layered clay, which are important minerals of soils and clay formations. This knowledge is mandatory to better understand / predict the surface reactivity of clays and its impact on the behavior of TME in agricultural water-soil systems, or in assessing the safety of high-level radioactive waste disposal in clay rocks. This work also provides a context for more in-depth spectroscopic studies of complex ternary systems of TME/radionuclides, phosphates, clays and solutions.

Acknowledgments

We thank for analyses of clay samples: ITES (Institut Terre et Environnement de Strasbourg, Strasbourg University, France) for mineralogical analyses, SARM-CRPG (Service d'Analyse des Roches et Minéraux, Centre de Recherches Pétrographiques et Géochimiques, Nancy, France) for major element and trace element analysis, and ECPM (École de Chimie des Polymères et Matériaux, Strasbourg, France) for BET measurements. We are grateful to the A. Boos for giving us access to the ICP-OES and ICP-MS equipments of the "Plateforme des Inorganiques" of IPHC for our solution analyses. We are very grateful to three anonymous reviewers and to the Editor, Professor Robert Tilton, for their constructive comments, which improved the manuscript considerably.

Funding

This research work was funded by the European Commission in the frame of the European Joint Programme on Radioactive Waste Management EURAD (Grant agreement ID 847593, contract number CNRS 198255) and took place in the Work Package FUTURE of EURAD.

Appendix A. Supporting information

References

[1] S. Goldberg, G. Sposito, A Chemical Model of Phosphate Adsorption by Soils: II. Noncalcareous Soils, Soil Science Society of America Journal. 48 (1984) 779–783. https://doi.org/10.2136/sssaj1984.03615995004800040016x.

[2] R.L. Parfitt, R.J. Atkinson, Phosphate adsorption on goethite (α-FeOOOH), Nature. 264 (1976) 740–742. https://doi.org/10.1038/264740a0.

[3] M.I. Tejedor-Tejedor, M.A. Anderson, The protonation of phosphate on the surface of goethite as studied by CIR-FTIR and electrophoretic mobility, Langmuir. 6 (1990) 602–611. https://doi.org/10.1021/la00093a015.

[4] C. Luengo, M. Brigante, J. Antelo, M. Avena, Kinetics of phosphate adsorption on goethite: Comparing batch adsorption and ATR-IR measurements, Journal of Colloid and Interface Science. 300 (2006) 511–518. https://doi.org/10.1016/j.jcis.2006.04.015.

[5] D.B. Abdala, P.A. Northrup, Y. Arai, D.L. Sparks, Surface loading effects on orthophosphate surface complexation at the goethite/water interface as examined by extended X-ray Absorption Fine Structure (EXAFS) spectroscopy, Journal of Colloid and Interface Science. 437 (2015) 297–303. https://doi.org/10.1016/j.jcis.2014.09.057.

[6] Y. Arai, D.L. Sparks, ATR–FTIR Spectroscopic Investigation on Phosphate Adsorption Mechanisms at the Ferrihydrite–Water Interface, Journal of Colloid and Interface Science. 241 (2001) 317–326. https://doi.org/10.1006/jcis.2001.7773.

[7] E.J. Elzinga, D.L. Sparks, Phosphate adsorption onto hematite: An in situ ATR-FTIR investigation of the effects of pH and loading level on the mode of phosphate surface complexation, Journal of Colloid and Interface Science. 308 (2007) 53–70. https://doi.org/10.1016/j.jcis.2006.12.061.

[8] M. Del Nero, C. Galindo, R. Barillon, E. Halter, B. Madé, Surface reactivity of α-Al2O3 and mechanisms of phosphate sorption: In situ ATR-FTIR spectroscopy and ζ potential studies, Journal of Colloid and Interface Science. 342 (2010) 437–444. https://doi.org/10.1016/j.jcis.2009.10.057.

[9] W. Li, A.-M. Pierre-Louis, K.D. Kwon, J.D. Kubicki, D.R. Strongin, B.L. Phillips, Molecular level investigations of phosphate sorption on corundum (α-Al2O3) by 31P solid state NMR, ATR-FTIR and quantum chemical calculation, Geochimica et Cosmochimica Acta. 107 (2013) 252–266. https://doi.org/10.1016/j.gca.2013.01.007.

[10] T. Roy, D. Wisser, M. Rivallan, M.C. Valero, T. Corre, O. Delpoux, G.D. Pirngruber, G. Lefèvre, Phosphate Adsorption on γ-Alumina: A Surface Complex Model Based on Surface Characterization and Zeta Potential Measurements, J. Phys. Chem. C. (2021) acs.jpcc.0c11553. https://doi.org/10.1021/acs.jpcc.0c11553.

[11] R.J. Atkinson, R.L. Parfitt, R.St.C. Smart, Infra-red study of phosphate adsorption on goethite, J. Chem. Soc., Faraday Trans. 1. 70 (1974) 1472. https://doi.org/10.1039/f19747001472.

[12] Y.S.R. Chen, J.N. Butler, Werner. Stumm, Kinetic study of phosphate reaction with aluminum oxide and kaolinite, Environ. Sci. Technol. 7 (1973) 327–332. https://doi.org/10.1021/es60076a007.

[13] T.J. Van Emmerik, D.E. Sandström, O.N. Antzutkin, M.J. Angove, B.B. Johnson, ^{31} P Solid-State Nuclear Magnetic Resonance Study of the Sorption of Phosphate onto Gibbsite and Kaolinite, Langmuir. 23 (2007) 3205–3213. https://doi.org/10.1021/la062765b.

[14] Y.-S.R. Chen, J.N. Butler, W. Stumm, Adsorption of phosphate on alumina and kaolinite from dilute aqueous solutions, Journal of Colloid and Interface Science. 43 (1973) 421–436. https://doi.org/10.1016/0021-9797(73)90388-3.

[15] W.F. Bleam, P.E. Pfeffer, S. Goldberg, R.W. Taylor, R. Dudley, A phosphorus-31 solid-state nuclear magnetic resonance study of phosphate adsorption at the boehmite/aqueous solution interface, Langmuir. 7 (1991) 1702–1712. https://doi.org/10.1021/la00056a023.

[16] K.O. Adebowale, I.E. Unuabonah, B.I. Olu-Owolabi, Adsorption of some heavy metal ions on sulfate- and phosphate-modified kaolin, Applied Clay Science. 29 (2005) 145–148. https://doi.org/10.1016/j.clay.2004.10.003.
[17] D.L. Sparks, Environmental soil chemistry, Academic Press, Inc., San Diego, 1995.
[18] F. Gérard, Clay minerals, iron/aluminum oxides, and their contribution to phosphate sorption in soils — A myth revisited, Geoderma. 262 (2016) 213–226. https://doi.org/10.1016/j.geoderma.2015.08.036.
[19] M. Dolui, S. Rakshit, M.E. Essington, G. Lefèvre, Probing Oxytetracycline Sorption Mechanism on Kaolinite in a Single Ion and Binary Mixtures with Phosphate using In Situ ATR-FTIR Spectroscopy, Soil Science Society of America Journal. 82 (2018) 826–838. https://doi.org/10.2136/sssaj2018.01.0020.
[20] Y. Arai, Effects of Dissolved Calcium on Arsenate Sorption at the Kaolinite-Water Interface, Soil Science. 175 (2010) 207–213. https://doi.org/10.1097/SS.0b013e3181dd799d.
[21] Y. Arai, D.L. Sparks, J.A. Davis, Arsenate Adsorption Mechanisms at the Allophane−Water Interface, Environ. Sci. Technol. 39 (2005) 2537–2544. https://doi.org/10.1021/es0486770.
[22] J.K. Edzwald, D.C. Toensing, M.C.-Yew. Leung, Phosphate adsorption reactions with clay minerals, Environ. Sci. Technol. 10 (1976) 485–490. https://doi.org/10.1021/es60116a001.
[23] L. Borgnino, C.E. Giacomelli, M.J. Avena, C.P. De Pauli, Phosphate adsorbed on Fe(III) modified montmorillonite: Surface complexation studied by ATR-FTIR spectroscopy, Colloids and Surfaces A: Physicochemical and Engineering Aspects. 353 (2010) 238–244. https://doi.org/10.1016/j.colsurfa.2009.11.022.
[24] Y. Wang, M. Frutschi, E. Suvorova, V. Phrommavanh, M. Descostes, A.A.A. Osman, G. Geipel, R. Bernier-Latmani, Mobile uranium(IV)-bearing colloids in a mining-impacted wetland, Nat Commun. 4 (2013) 2942. https://doi.org/10.1038/ncomms3942.
[25] L. Stetten, P. Blanchart, A. Mangeret, P. Lefebvre, P. Le Pape, J. Brest, P. Merrot, A. Julien, O. Proux, S.M. Webb, J.R. Bargar, C. Cazala, G. Morin, Redox Fluctuations and Organic Complexation Govern Uranium Redistribution from U(IV)-Phosphate Minerals in a Mining-Polluted Wetland Soil, Brittany, France, Environ. Sci. Technol. 52 (2018) 13099–13109. https://doi.org/10.1021/acs.est.8b03031.
[26] V.R. Vermeul, B.N. Bjornstad, B.G. Fritz, J.S. Fruchter, R.D. Mackley, D.R. Newcomer, D.P. Mendoza, M.L. Rockhold, D.M. Wellman, M.D. Williams, 300 Area Uranium Stabilization Through Polyphosphate Injection: Final Report, 2009. https://doi.org/10.2172/967237.
[27] Z. Pan, D.E. Giammar, V. Mehta, L.D. Troyer, J.G. Catalano, Z. Wang, Phosphate-Induced Immobilization of Uranium in Hanford Sediments, Environ. Sci. Technol. 50 (2016) 13486–13494. https://doi.org/10.1021/acs.est.6b02928.
[28] G. Sposito, N.T. Skipper, R. Sutton, S. -h. Park, A.K. Soper, J.A. Greathouse, Surface geochemistry of the clay minerals, Proceedings of the National Academy of Sciences. 96 (1999) 3358–3364. https://doi.org/10.1073/pnas.96.7.3358.
[29] M. Marques Fernandes, B. Baeyens, R. Dähn, A.C. Scheinost, M.H. Bradbury, U(VI) sorption on montmorillonite in the absence and presence of carbonate: A macroscopic and microscopic study, Geochimica et Cosmochimica Acta. 93 (2012) 262–277. https://doi.org/10.1016/j.gca.2012.04.017.
[30] V. Montoya, B. Baeyens, M.A. Glaus, T. Kupcik, M. Marques Fernandes, L. Van Laer, C. Bruggeman, N. Maes, T. Schäfer, Sorption of Sr, Co and Zn on illite: Batch experiments and modelling including Co in-diffusion measurements on compacted samples, Geochimica et Cosmochimica Acta. 223 (2018) 1–20. https://doi.org/10.1016/j.gca.2017.11.027.
[31] G. Montavon, S. Ribet, Y.H. Loni, F. Maia, C. Bailly, K. David, C. Lerouge, B. Madé, J.C. Robinet, B. Grambow, Uranium retention in a Callovo-Oxfordian clay rock formation: From laboratory-based models to in natura conditions, Chemosphere. 299 (2022) 134307. https://doi.org/10.1016/j.chemosphere.2022.134307.

[32] R.H. Byrne, J.H. Lee, L.S. Bingler, Rare earth element complexation by PO43− ions in aqueous solution, Geochimica et Cosmochimica Acta. 55 (1991) 2729–2735. https://doi.org/10.1016/0016-7037(91)90439-C.
[33] A. Sandino, J. Bruno, The solubility of (UO2)3(PO4)2 4H20(s) and the formation of U(VI) phosphate complexes: Their influence in uranium speciation in natural waters, Geochimica et Cosmochimica Acta. 56 (1992) 4135–4145. https://doi.org/10.1016/0016-7037(92)90256-I.
[34] R. Guillaumont, T. Fanghänel, J. Fuger, I. Grenthe, V. Neck, D.A. Palmer, M.H. Rand, UPDATE ON THE CHEMICAL THERMODYNAMICS OF URANIUM, NEPTUNIUM, PLUTONIUM, AMERICIUM AND TECHNETIUM, OECD Nuclear Energy Agency; Elsevier: Amsterdam. (2003).
[35] K. Maher, J.R. Bargar, G.E. Brown, Environmental Speciation of Actinides, Inorg. Chem. 52 (2013) 3510–3532. https://doi.org/10.1021/ic301686d.
[36] S.A. Cumberland, G. Douglas, K. Grice, J.W. Moreau, Uranium mobility in organic matter-rich sediments: A review of geological and geochemical processes, Earth-Science Reviews. 159 (2016) 160–185. https://doi.org/10.1016/j.earscirev.2016.05.010.
[37] J. Bruno, L. Duro, M. Grivé, The applicability and limitations of thermodynamic geochemical models to simulate trace element behaviour in natural waters. Lessons learned from natural analogue studies, Chemical Geology. 190 (2002) 371–393. https://doi.org/10.1016/S0009-2541(02)00126-2.
[38] K.H. Johannesson, W.B. Lyons, K.J. Stetzenbach, R.H. Byrne, The solubility control of rare earth elements in natural terrestrial waters and the significance of PO 4 3? and CO 3 2? in limiting dissolved rare earth concentrations: A review of recent information, Aquat Geochem. 1 (1995) 157–173. https://doi.org/10.1007/BF00702889.
[39] D. Gorman-Lewis, T. Shvareva, K.-A. Kubatko, P.C. Burns, D.M. Wellman, B. McNamara, J.E.S. Szymanowski, A. Navrotsky, J.B. Fein, Thermodynamic Properties of Autunite, Uranyl Hydrogen Phosphate, and Uranyl Orthophosphate from Solubility and Calorimetric Measurements, Environ. Sci. Technol. 43 (2009) 7416–7422. https://doi.org/10.1021/es9012933.
[40] M.F. Fanizza, H. Yoon, C. Zhang, M. Oostrom, T.W. Wietsma, N.J. Hess, M.E. Bowden, T.J. Strathmann, K.T. Finneran, C.J. Werth, Pore-scale evaluation of uranyl phosphate precipitation in a model groundwater system, Water Resources Research. 49 (2013) 874–890. https://doi.org/10.1002/wrcr.20088.
[41] M. Kanematsu, N. Perdrial, W. Um, J. Chorover, P.A. O'Day, Influence of Phosphate and Silica on U(VI) Precipitation from Acidic and Neutralized Wastewaters, Environ. Sci. Technol. 48 (2014) 6097–6106. https://doi.org/10.1021/es4056559.
[42] V.S. Mehta, F. Maillot, Z. Wang, J.G. Catalano, D.E. Giammar, Effect of co-solutes on the products and solubility of uranium(VI) precipitated with phosphate, Chemical Geology. 364 (2014) 66–75. https://doi.org/10.1016/j.chemgeo.2013.12.002.
[43] W. Um, Z. Wang, R.J. Serne, B.D. Williams, C.F. Brown, C.J. Dodge, A.J. Francis, Uranium Phases in Contaminated Sediments below Hanford's U Tank Farm, Environ. Sci. Technol. 43 (2009) 4280–4286. https://doi.org/10.1021/es900203r.
[44] T.E. Payne, G.R. Lumpkin, T.D. Waite, Uranium{sup VI} adsorption on model minerals. Controlling factors and surface complexation modeling. Chapter 2, (1998). https://www.osti.gov/etdeweb/biblio/20232360 (accessed March 30, 2023).
[45] M. Del Nero, C. Galindo, R. Barillon, B. Madé, TRLFS Evidence for Precipitation of Uranyl Phosphate on the Surface of Alumina: Environmental Implications, Environ. Sci. Technol. 45 (2011) 3982–3988. https://doi.org/10.1021/es2000479.
[46] L.D. Troyer, F. Maillot, Z. Wang, Z. Wang, V.S. Mehta, D.E. Giammar, J.G. Catalano, Effect of phosphate on U(VI) sorption to montmorillonite: Ternary complexation and precipitation barriers, Geochimica et Cosmochimica Acta. 175 (2016) 86–99. https://doi.org/10.1016/j.gca.2015.11.029.
[47] A. Gładysz-Płaska, E. Grabias, M. Majdan, Simultaneous adsorption of uranium(VI) and phosphate on red clay, Progress in Nuclear Energy. 104 (2018) 150–159. https://doi.org/10.1016/j.pnucene.2017.09.010.

[48] L. Dithmer, A.S. Lipton, K. Reitzel, T.E. Warner, D. Lundberg, U.G. Nielsen, Characterization of Phosphate Sequestration by a Lanthanum Modified Bentonite Clay: A Solid-State NMR, EXAFS, and PXRD Study, Environ. Sci. Technol. 49 (2015) 4559–4566. https://doi.org/10.1021/es506182s.
[49] R. Finch, T. Murakami, 3. Systematics and Paragenesis of Uranium Minerals, in: P.C. Burns, R.J. Finch (Eds.), Uranium, De Gruyter, 1999: pp. 91–180. https://doi.org/10.1515/9781501509193-008.
[50] D.E. Morris, P.G. Allen, J.M. Berg, C.J. Chisholm-Brause, S.D. Conradson, R.J. Donohoe, N.J. Hess, J.A. Musgrave, C.D. Tait, Speciation of Uranium in Fernald Soils by Molecular Spectroscopic Methods: Characterization of Untreated Soils, Environ. Sci. Technol. 30 (1996) 2322–2331. https://doi.org/10.1021/es950745i.
[51] J.L. Jerden, A.K. Sinha, Phosphate based immobilization of uranium in an oxidizing bedrock aquifer, Applied Geochemistry. 18 (2003) 823–843. https://doi.org/10.1016/S0883-2927(02)00179-8.
[52] J.L. Jerden, A.K. Sinha, Geochemical coupling of uranium and phosphorous in soils overlying an unmined uranium deposit: Coles Hill, Virginia, Journal of Geochemical Exploration. 91 (2006) 56–70. https://doi.org/10.1016/j.gexplo.2005.12.003.
[53] J.L. Jerden, A.K. Sinha, L. Zelazny, Natural immobilization of uranium by phosphate mineralization in an oxidizing saprolite–soil profile: chemical weathering of the Coles Hill uranium deposit, Virginia, Chemical Geology. 199 (2003) 129–157. https://doi.org/10.1016/S0009-2541(03)00080-9.
[54] J.G. Catalano, J.P. McKinley, J.M. Zachara, S.M. Heald, S.C. Smith, G.E. Brown, Changes in Uranium Speciation through a Depth Sequence of Contaminated Hanford Sediments, Environ. Sci. Technol. 40 (2006) 2517–2524. https://doi.org/10.1021/es0520969.
[55] D.M. Singer, J.M. Zachara, G.E. Brown Jr, Uranium Speciation As a Function of Depth in Contaminated Hanford Sediments - A Micro-XRF, Micro-XRD, and Micro- And Bulk-XAFS Study, Environ. Sci. Technol. 43 (2009) 630–636. https://doi.org/10.1021/es8021045.
[56] J.E. Stubbs, L.A. Veblen, D.C. Elbert, J.M. Zachara, J.A. Davis, D.R. Veblen, Newly recognized hosts for uranium in the Hanford Site vadose zone, Geochimica et Cosmochimica Acta. 73 (2009) 1563–1576. https://doi.org/10.1016/j.gca.2008.12.004.
[57] A.J. Pinto, M.A. Gonçalves, C. Prazeres, J.M. Astilleros, M.J. Batista, Mineral replacement reactions in naturally occurring hydrated uranyl phosphates from the Tarabau deposit: Examples in the Cu–Ba uranyl phosphate system, Chemical Geology. 312–313 (2012) 18–26. https://doi.org/10.1016/j.chemgeo.2012.04.004.
[58] Y. Arai, M.A. Marcus, N. Tamura, J.A. Davis, J.M. Zachara, Spectroscopic Evidence for Uranium Bearing Precipitates in Vadose Zone Sediments at the Hanford 300-Area Site, Environ. Sci. Technol. 41 (2007) 4633–4639. https://doi.org/10.1021/es062196u.
[59] J. Bruno, J. De Pablo, L. Duro, E. Figuerola, Experimental study and modeling of the U(VI)-Fe(OH)3 surface precipitation/coprecipitation equilibria, Geochimica et Cosmochimica Acta. 59 (1995) 4113–4123. https://doi.org/10.1016/0016-7037(95)00243-S.
[60] M. Del Nero, S. Salah, T. Miura, A. Clément, F. Gauthier-Lafaye, Sorption/Desorption Processes of Uranium in Clayey Samples of the Bangombe Natural Reactor Zone, Gabon, Radiochimica Acta. 87 (1999) 135–150. https://doi.org/10.1524/ract.1999.87.34.135.
[61] M. Del Nero, A. Froideval, C. Gaillard, G. Mignot, R. Barillon, I. Munier, A. Ozgümüs, Mechanisms of uranyl sorption, Geological Society, London, Special Publications. 236 (2004) 545–560. https://doi.org/10.1144/GSL.SP.2004.236.01.30.
[62] M.M.S. Cabral Pinto, M.M.V.G. Silva, A.M.R. Neiva, Release, Migration, Sorption and (re)precipitation of U During a Granite Alteration under Oxidizing Conditions, Procedia Earth and Planetary Science. 8 (2014) 28–32. https://doi.org/10.1016/j.proeps.2014.05.007.
[63] M. Edahbi, B. Plante, M. Benzaazoua, M. Ward, M. Pelletier, Mobility of rare earth elements in mine drainage: Influence of iron oxides, carbonates, and phosphates, Chemosphere. 199 (2018) 647–654. https://doi.org/10.1016/j.chemosphere.2018.02.054.

[64] Md.S. Alam, T. Cheng, Uranium release from sediment to groundwater: Influence of water chemistry and insights into release mechanisms, Journal of Contaminant Hydrology. 164 (2014) 72–87. https://doi.org/10.1016/j.jconhyd.2014.06.001.
[65] S. Salah, F. Gauthier-Lafaye, M. Del Nero, G. Le Bricon, G. Bracke, Behavior of REE in the Weathering Sequence of the Natural Fission Reactor at Bangombe (Oklo)., In: Abstr. of the Int. Conf. European Union of Geosciences EUG 10, Strasbourg, France,. (1999).
[66] M. Del Nero, C. Galindo, G. Bucher, S. Georg, V. Mazan, R. Barillon, Speciation of oxalate at corundum colloid–solution interfaces and its effect on colloid aggregation under conditions relevant to freshwaters, Colloids and Surfaces A: Physicochemical and Engineering Aspects. 418 (2013) 165–173. https://doi.org/10.1016/j.colsurfa.2012.11.011.
[67] T.E. Payne, G.R. Lumpkin, T.D. Waite, Uranium (VI) Adsorption on Model Minerals: Controlling factors and surface complexation modelling, (1996).
[68] Y. Arai, D.L. Sparks, Phosphate Reaction Dynamics in Soils and Soil Components: A Multiscale Approach, in: Advances in Agronomy, Elsevier, 2007: pp. 135–179. https://doi.org/10.1016/S0065-2113(06)94003-6.
[69] W. Li, A.-M. Pierre-Louis, K.D. Kwon, J.D. Kubicki, D.R. Strongin, B.L. Phillips, Molecular level investigations of phosphate sorption on corundum (α-Al2O3) by 31P solid state NMR, ATR-FTIR and quantum chemical calculation, Geochimica et Cosmochimica Acta. 107 (2013) 252–266. https://doi.org/10.1016/j.gca.2013.01.007.
[70] M. Del Nero, C. Galindo, R. Barillon, E. Halter, B. Madé, Surface reactivity of α-Al2O3 and mechanisms of phosphate sorption: In situ ATR-FTIR spectroscopy and ζ potential studies, Journal of Colloid and Interface Science. 342 (2010) 437–444. https://doi.org/10.1016/j.jcis.2009.10.057.
[71] T. Roy, D. Wisser, M. Rivallan, M.C. Valero, T. Corre, O. Delpoux, G.D. Pirngruber, G. Lefèvre, Phosphate Adsorption on γ-Alumina: A Surface Complex Model Based on Surface Characterization and Zeta Potential Measurements, J. Phys. Chem. C. (2021) acs.jpcc.0c11553. https://doi.org/10.1021/acs.jpcc.0c11553.
[72] G. Lefèvre, In situ Fourier-transform infrared spectroscopy studies of inorganic ions adsorption on metal oxides and hydroxides, Advances in Colloid and Interface Science. 107 (2004) 109–123. https://doi.org/10.1016/j.cis.2003.11.002.
[73] C. Galindo, M.D. Nero, R. Barillon, E. Halter, B. Made, Mechanisms of uranyl and phosphate (co)sorption: Complexation and precipitation at α-Al2O3 surfaces, Journal of Colloid and Interface Science. 347 (2010) 282–289. https://doi.org/10.1016/j.jcis.2010.03.045.
[74] M.A. Glaus, M. Aertsens, N. Maes, L. Van Laer, L.R. Van Loon, Treatment of boundary conditions in through-diffusion: A case study of 85Sr2+ diffusion in compacted illite, Journal of Contaminant Hydrology. 177–178 (2015) 239–248. https://doi.org/10.1016/j.jconhyd.2015.03.010.
[75] V. Bout-Roumazeilles, E. Cortijo, L. Labeyrie, P. Debrabant, Clay mineral evidence of nepheloid layer contributions to the Heinrich layers in the northwest Atlantic, Palaeogeography, Palaeoclimatology, Palaeoecology. 146 (1999) 211–228.
[76] G.W. Brindley, G. Brown, Crystal Structures of Clay Minerals and Their X-ray Identification., Mineralogical Society, 1980.
[77] M.H. Bradbury, B. Baeyens, Sorption modelling on illite Part I: Titration measurements and the sorption of Ni, Co, Eu and Sn, Geochimica et Cosmochimica Acta. 73 (2009) 990–1003. https://doi.org/10.1016/j.gca.2008.11.017.
[78] P. Persson, N. Nilsson, S. Sjöberg, Structure and Bonding of Orthophosphate Ions at the Iron Oxide–Aqueous Interface, Journal of Colloid and Interface Science. 177 (1996) 263–275. https://doi.org/10.1006/jcis.1996.0030.
[79] C. Poinssot, B. Baeyens, M.H. Bradbury, Experimental and modelling studies of caesium sorption on illite, Geochimica et Cosmochimica Acta. 63 (1999) 3217–3227. https://doi.org/10.1016/S0016-7037(99)00246-X.

[80] G. Sposito, The surface chemistry of soils, Oxford University Press ; Clarendon Press, New York : Oxford [Oxfordshire], 1984.
[81] J.A. Davis, D.B. Kent, CHAPTER 5. SURFACE COMPLEXATION MODELING IN AQUEOUS GEOCHEMISTRY, in: M.F. Hochella, A.F. White (Eds.), Mineral-Water Interface Geochemistry, De Gruyter, 1990: pp. 177–260. https://doi.org/10.1515/9781501509131-009.
[82] Q. Du, Z. Sun, W. Forsling, H. Tang, Acid-Base Properties of Aqueous Illite Surfaces, (1996).
[83] G.M. Beene, R. Bryant, D.J.A. Williams, Electrochemical properties of illites, Journal of Colloid and Interface Science. 147 (1991) 358–369. https://doi.org/10.1016/0021-9797(91)90168-8.
[84] J. Madejová, Baseline Studies of the Clay Minerals Society Source Clays: Infrared Methods, Clays and Clay Minerals. 49 (2001) 410–432. https://doi.org/10.1346/CCMN.2001.0490508.
[85] D. Vantelon, M. Pelletier, L.J. Michot, O. Barres, F. Thomas, Fe, Mg and Al distribution in the octahedral sheet of montmorillonites. An infrared study in the OH- bending region, Clay Miner. 36 (2001) 369–379. https://doi.org/10.1180/000985501750539463.
[86] C.T. Johnston, G.S. Premachandra, Polarized ATR-FTIR Study of Smectite in Aqueous Suspension, Langmuir. 17 (2001) 3712–3718. https://doi.org/10.1021/la010184a.
[87] R. Ellerbrock, M. Stein, J. Schaller, Comparing amorphous silica, short-range-ordered silicates and silicic acid species by FTIR, Sci Rep. 12 (2022) 11708. https://doi.org/10.1038/s41598-022-15882-4.
[88] M. Ritz, L. Vaculíková, E. Plevová, APPLICATION OF INFRARED SPECTROSCOPY AND CHEMOMETRIC METHODS TO IDENTIFICATION OF SELECTED MINERALS, Acta Geodynamica et Geromaterialia. 8 (2011) 47–58.
[89] R.J. Hunter, Electroviscous and Viscoelectric Effects, in: Zeta Potential in Colloid Science, Elsevier, 1981: pp. 179–218. https://doi.org/10.1016/B978-0-12-361961-7.50009-2.
[90] R.J. Hunter, A.E. Alexander, Surface properties and flow behavior of kaolinite. Part I: Electrophoretic mobility and stability of kaolinite sols, Journal of Colloid Science. 18 (1963) 820–832. https://doi.org/10.1016/0095-8522(63)90076-X.
[91] K. Nakamoto, Infrared and Raman Spectra of Inorganic and Coordination Compounds, Handbook of Vibrational Spectroscopy. (2006) 21.